

# Novel approach to pion and eta production in proton-proton collisions near threshold<sup>#1</sup>

V. Bernard<sup>‡</sup>, N. Kaiser<sup>◇</sup>, Ulf-G. Meißner<sup>†</sup>

<sup>‡</sup>Université Louis Pasteur, Laboratoire de Physique Théorique  
3-5, rue de l'Université, F-67084 Strasbourg, France  
*email: bernard@lpt1.u-strasbg.fr*

<sup>◇</sup>Technische Universität München, Physik Department T39  
James-Franck-Straße, D-85747 Garching, Germany  
*email: nkaiser@physik.tu-muenchen.de*

<sup>†</sup>Forschungszentrum Jülich, Institut für Kernphysik (Theorie)  
D-52425 Jülich, Germany  
*email: Ulf-G.Meissner@fz-juelich.de*

## Abstract

We evaluate the threshold matrix-element for the reaction  $pp \rightarrow pp\pi^0$  in a fully relativistic Feynman diagrammatic approach. We employ a simple effective range approximation to take care of the S-wave final-state interaction. The experimental value for the threshold amplitude  $\mathcal{A} = (2.7 - i0.3) \text{ fm}^4$  can be reproduced by contributions from tree level chiral (long-range) pion exchange and short-range effects related to vector meson exchanges, with  $\omega$  exchange giving the largest individual contribution. Pion loop effects appear to be small. We stress that the commonly used heavy baryon formalism is not applicable in the NN-system above the pion production threshold due to the large external momentum,  $|\vec{p}| \simeq \sqrt{Mm_\pi}$ , with  $M$  and  $m_\pi$  the nucleon and the pion mass, respectively. We furthermore investigate the reaction  $pp \rightarrow pn\pi^+$  near threshold within the same approach. We extract from the data the triplet threshold amplitude as  $\mathcal{B} = (2.8 - i1.5) \text{ fm}^4$ . Its real part can be well understood from (relativistic) tree level meson-exchange diagrams. In addition, we investigate the process  $pp \rightarrow pp\eta$  near threshold. We use a simple factorization ansatz for the  $pp\eta$  final-state interaction and extract from the data the modulus of the threshold amplitude,  $|\mathcal{C}| = 1.32 \text{ fm}^4$ . With  $g_{\eta N} = 5.3$ , this value can be reproduced by (relativistic) tree level meson-exchange diagrams and  $\eta$ -rescattering, whose strength is fixed by the  $\eta N$  scattering length. We also comment on the recent near threshold data for  $\eta'$ -production.

---

<sup>#1</sup>Work supported by DFG under contract no. 445 AUS-113/3/0.

# 1 Introduction and summary

With the advent of proton cooler synchrotrons at Bloomington, Jülich and Uppsala, high precision data for the processes  $pp \rightarrow pp\pi^0$ ,  $pp \rightarrow d\pi^+$ ,  $pp \rightarrow pn\pi^+$  and  $pp \rightarrow pp\eta$  in the threshold region [1, 2, 3, 4, 5] have become available. The first data on neutral pion production were a big surprise because the experimental cross sections turned out to be a factor of five larger than the theoretical predictions based on direct pion production and neutral pion rescattering fixed from on-shell  $\pi N$  data. Nevertheless, the energy-dependence of the total cross section  $\sigma_{\text{tot}}$  from threshold to excess energies of about 50 MeV is completely given by the strong S-wave  $pp$  final-state interaction, see e.g. ref.[6]. Subsequently, it was argued that heavy-meson exchanges might be able to remove this discrepancy [7, 8]. On the other hand it was shown [9, 10] that the (model-dependent) off-shell behavior of the full  $\pi N$  T-matrix also can enhance the cross section considerably. Another avenue to eventually understand the near threshold cross section is offered by calculations within the framework of tree-level heavy baryon chiral perturbation theory (HBChPT) including dimension two operators [11, 12, 13, 14]. In these papers, HBChPT has been used to constrain the long-range  $\pi^0$ -exchange contributions. However, it was found that the calculations for  $pp \rightarrow pp\pi^0$  performed so far lead to a marked difference in the role of the so-called  $\pi^0$  rescattering contribution, which interferes constructively with the direct production in the Jülich model and destructively in the HBChPT framework, respectively. In a recent paper, it was argued that the treatment underlying the isoscalar pion-nucleon scattering amplitude and the related transition operator for the process  $NN \rightarrow NN\pi$  (where  $N$  denotes the nucleon) in the HBChPT framework is not yet sufficiently accurate and thus the resulting rescattering contribution should be considered as an artifact of this approximation [15]. It was also stressed that the process  $pp \rightarrow d\pi^+$  is more sensitive to the long-range (chiral) pion exchange. One-loop graphs have been considered in [16].

However, one important feature of this reaction should be kept in mind, namely the large momentum mismatch between the initial and the final nucleon-nucleon state: the initial center-of-mass momentum is given by  $|\vec{p}|^2 = Mm_\pi + m_\pi^2/4$ , with  $m_\pi$  ( $M$ ) the neutral pion (proton) mass, whereas close to threshold the final one is compatible with zero. This large difference leads to momentum transfers equal to  $|\vec{p}|$  and higher. In particular, both the squared invariant momentum transfer and the kinetic energy of the incoming protons are  $-Mm_\pi$  and  $m_\pi/2$ , respectively, and therefore the chiral counting in the original sense does not apply, see e.g. [12]. We will actually demonstrate here that non-relativistic approximations (i.e. the heavy baryon formalism or HBChPT) are not applicable in the two-nucleon system above the pion production threshold. The simple reason for that is the extreme kinematics with the external momentum  $|\vec{p}| \simeq \sqrt{Mm_\pi}$  diverging in the heavy nucleon limit  $M \rightarrow \infty$  (while this argument could be considered formal, it nicely pinpoints the problems of the heavy baryon approach). The HBChPT framework (which is very successful for low-energy single nucleon processes) loses its systematic order-by-order low-energy expansion when external momenta grow with the nucleon mass ( $|\vec{p}| \sim \sqrt{M}$ ). In order to avoid such problems (which are simply related to kinematics) it seems mandatory to perform fully relativistic calculations. In particular, we find that one of the low-energy constants  $c_2$  entering the chiral  $\pi^0$ -rescattering is enhanced in the relativistic calculation by a factor of two as compared to the non-relativistic HBChPT approach. In this spirit we perform here a fully relativistic calculation of various tree and one-loop diagrams contributing to  $pp \rightarrow pp\pi^0$  and  $pp \rightarrow pn\pi^+$  at threshold. Our approach can also be extended in a straightforward manner to  $\eta$  and  $\eta'$  production in  $pp$ -collisions. We thus discuss here also the reaction  $pp \rightarrow pp\eta$  up to laboratory excess energies of about 100 MeV using a simple factorized form to account for the final-state interactions in the  $pp\eta$  three-body system.

The pertinent results of this investigation can be summarized as follows:

- (i) Assuming that the  $pp$  final-state interaction is an on-shell NN-process and using a simple effective range parametrization for the  $^1S_0$   $pp$  phase shift, we can accurately fit the 40 data points of the total cross section from threshold up to  $T_{\text{lab}} = 326$  MeV with a constant (threshold) amplitude equal to  $\mathcal{A} = (2.7 - i0.3)$  fm<sup>4</sup>.
- (ii) The real part of this number can be well understood in terms of chiral  $\pi^0$  exchange (including chiral  $\pi^0$  rescattering) and heavy meson ( $\omega, \rho^0, \eta$ ) exchanges based on a relativistic Feynman diagram calculation.
- (iii) We have evaluated some classes of one-loop graphs and find that they lead to small corrections of the order of a few percent. Therefore chiral loops do not seem to play any significant role in the processes  $NN \rightarrow NN\pi$ , which are dominated by one-pion exchange and short-range physics (with the notable exception of  $pp \rightarrow d\pi^+$ , where  $d$  denotes the deuteron).
- (iv) Both the long range  $\pi^0$  exchange and the short range vector meson exchange lead to contributions to the threshold amplitude  $\mathcal{A}$  which do not vanish in the chiral limit  $m_\pi \rightarrow 0$ . There is no chiral suppression of the reaction  $pp \rightarrow pp\pi^0$  compared to other  $NN\pi$  channels. In all cases the respective threshold amplitudes are non-zero (and finite) in the chiral limit. This is in contrast to the widespread believe that  $pp \rightarrow pp\pi^0$  is suppressed for reasons of chiral symmetry.
- (v) Within the same approach, we have investigated the threshold behavior of the process  $pp \rightarrow pn\pi^+$ . It is given in terms of  $\mathcal{A}$  and the triplet threshold amplitude  $\mathcal{B}$  with the empirical value  $\mathcal{B} = (2.8 - i1.5)$  fm<sup>4</sup>. The corresponding real part  $\text{Re}\mathcal{B}$  is well reproduced by chiral one-pion exchange and short-range vector meson physics. The empirical value of  $\mathcal{B}$  has however a sizeable imaginary part, which naturally can not be explained by tree graphs. This channel deserves some further study. The small and large imaginary parts of  $\mathcal{A}$  and  $\mathcal{B}$ , respectively, are related to the weak and strong initial state interaction in the  $^3P_0$  and  $^3P_1$  entrance channel, respectively.
- (vi) Finally, we have investigated the process  $pp \rightarrow pp\eta$  near threshold. We treat the final state-interaction in the  $pp$  and  $\eta p$  subsystems using a factorization ansatz and effective range approximations. The empirical value of the modulus of the threshold amplitude,  $|\mathcal{C}| = 1.32$  fm<sup>4</sup>, is reproduced with  $g_{\eta N} = 5.3$  by tree level meson exchange graphs and  $\eta$ -rescattering. The strength of the latter is fixed from the (real part of the)  $\eta N$  scattering length.
- (vii) Altogether, it is quite surprising that the total cross sections for pion and eta production in  $pp$ -collisions near threshold can be explained so simply in terms of final-state interaction (using effective range approximations) and certain well-known (relativistic) meson-exchange diagrams for the respective threshold amplitudes. However, such an approach requires further improvements and tests. First, one should include systematically initial-state and final-state NN-interactions. Secondly, in order to perform a detailed test of the underlying meson production mechanism one has to consider more exclusive observables like angular distributions of differential cross sections and asymmetries generated by polarized proton beams and targets. We hope to report on these topics in the near future.

## 2 Threshold kinematics and final–state interaction

### 2.1 Kinematics

We consider the reaction  $p_1(\vec{p}) + p_2(-\vec{p}) \rightarrow p + p + \pi^0$  in the center–of–mass (cm) frame at threshold (see fig. 1). The invariant T–matrix can be expressed in terms of one complex–valued (constant) amplitude, which we denote by  $\mathcal{A}$ , as

$$T_{\text{th}}^{\text{cm}}(pp \rightarrow pp\pi^0) = \mathcal{A} (i\vec{\sigma}_1 - i\vec{\sigma}_2 + \vec{\sigma}_1 \times \vec{\sigma}_2) \cdot \vec{p} \quad . \quad (1)$$

The  $\vec{\sigma}_{1,2}$  are the spin–matrices of the two protons. The value of the proton cm momentum to produce a neutral pion at rest is given by

$$|\vec{p}| = \sqrt{m_\pi(M + m_\pi/4)} = 362.2 \text{ MeV} \quad , \quad (2)$$

with  $M = 938.27$  MeV the proton and  $m_\pi = 134.97$  MeV the neutral pion mass, respectively. Obviously,  $|\vec{p}|$  vanishes in the chiral limit of zero pion mass. Therefore the soft–pion theorem which requires a vanishing threshold T–matrix in the chiral limit  $m_\pi = 0$  is trivially fulfilled (as long as  $\mathcal{A}$  does not become singular) [17]. We remark that similar features occur for the reaction  $\pi N \rightarrow \pi\pi N$  (see ref.[18]). All dynamical information is encoded in the threshold amplitude  $\mathcal{A}$  of dimension  $[\text{length}^4]$ . In the threshold region, the wave function of the final di–proton system as well as that of the neutral pion are dominated by angular momentum zero states, thus we are dealing with a  ${}^3P_0 \rightarrow {}^1S_0s$  transition. Consequently, one deduces from unitarity

$$\mathcal{A} = |\mathcal{A}| e^{i\delta({}^3P_0)} \quad , \quad (3)$$

with the  ${}^3P_0$   $pp$  phase shift to be taken at the threshold energy in the lab frame,  $T_{\text{th}}^{\text{lab}} = m_\pi(2 + m_\pi/2M) = 279.65$  MeV, where  $\delta({}^3P_0) = -6.3^\circ$  (FA95 solution of VPI). Thus the imaginary part  $\text{Im } \mathcal{A}$  is about  $-1/9$  of the real part  $\text{Re } \mathcal{A}$  and contributes negligibly to the total cross section near threshold proportional to  $|\mathcal{A}|^2$ . The threshold T–matrix is a pseudoscalar, it is symmetric under the exchange of the two ingoing protons  $\vec{\sigma}_1 \leftrightarrow \vec{\sigma}_2$ ,  $\vec{p} \rightarrow -\vec{p}$ . Furthermore Eq.(1) incorporates the Pauli exclusion principle for the (indistinguishable) outgoing protons, since left multiplication with the spin exchange operator  $(1 + \vec{\sigma}_1 \cdot \vec{\sigma}_2)/2$  leads to a minus sign by the identity:  $\frac{1}{2}(1 + \vec{\sigma}_1 \cdot \vec{\sigma}_2)(i\vec{\sigma}_1 - i\vec{\sigma}_2, \vec{\sigma}_1 \times \vec{\sigma}_2) = -(\vec{\sigma}_1 \times \vec{\sigma}_2, i\vec{\sigma}_1 - i\vec{\sigma}_2)$ . Diagrams with crossed proton lines are therefore automatically included. Approximating the near threshold T–matrix by the T–matrix exactly at threshold one gets for the unpolarized total cross section

$$\sigma_{\text{tot}}(T_{\text{lab}}) = \frac{M^4 \mu \sqrt{4 + \mu}}{16\pi^2 (2 + \mu)^{9/2}} |\mathcal{A}|^2 (T_{\text{lab}} - T_{\text{lab}}^{\text{th}})^2 \quad , \quad (4)$$

with  $\mu = m_\pi/M$ . Note that the flux and three–body phase space factors have been approximated in Eq.(4) by an analytical expression which is accurate within a few percent in the threshold region. Such a form has already been proven to be quite accurate in chiral perturbation theory studies of the reactions  $\gamma p \rightarrow \pi^0 \pi^0 p$  [19] and  $\pi N \rightarrow \pi\pi N$  [20], where  $\gamma$  denotes a real photon. In the case of  $pp \rightarrow pp\pi^0$ , however, such an approximation is not sufficient near threshold. This can be seen e.g. by taking the near threshold data of refs. [1, 2] and dividing them by the three–body phase space factor  $\sim (T_{\text{lab}} - T_{\text{lab}}^{\text{th}})^2$ , i.e.  $\sigma_{\text{tot}}(T_{\text{lab}}) = C \cdot (T_{\text{lab}} - T_{\text{lab}}^{\text{th}})^2$ . The resulting values for  $C$  are not constant in energy. This, of course, has to do with the strong  $pp$  final–state interaction in the  ${}^1S_0$  partial wave. So before we can extract a value for  $|\mathcal{A}|$ , we have to correct for the final–state interaction.

## 2.2 Treatment of the final–state interaction

The final–state interaction in the  $^1S_0$  di–proton state modifies the simple phase–space formula Eq.(4). We follow here a procedure derived by Watson [21] where one essentially assumes that final–state interaction is taking place only when the nucleons are on their mass–shell. In this approach, the unpolarized total cross section for  $pp \rightarrow pp\pi^0$  including final–state interaction takes the form

$$\begin{aligned} \sigma_{\text{tot}}(T_{\text{lab}}) &= |\mathcal{A}|^2 \left(\frac{M}{4\pi}\right)^3 \frac{2\sqrt{T_{\text{lab}}}}{(2M + T_{\text{lab}})^{3/2}} \\ &\times \int_{2M}^{W_{\text{max}}} dW \sqrt{(W^2 - 4M^2) \lambda(W^2, m_\pi^2, 4M^2 + 2MT_{\text{lab}})} F_p(W). \end{aligned} \quad (5)$$

Here,  $F_p(W)$  is the correction factor due the final–state interaction. We evaluate it in the effective range approximation. This is of course a very strong assumption but it allows to explain the energy dependence of the experimental total cross sections very accurately in terms of a single constant amplitude  $\mathcal{A}$ . Separating off the final–state interaction in that way, we can then pursue a diagrammatic approach to the (on-shell) production amplitude  $\mathcal{A}$ . This will allow us to investigate in a simple fashion the role of one-pion exchange and chiral loop effects together with shorter range exchanges due to heavier mesons. For a more complete dynamical description including off-shell final–state interactions and so on, a microscopic model treating also (unobservable) half-off shell effects is needed. After these remarks, we return to the effective range approximation, in which the function  $F_p(W)$  takes the form

$$F_p(W) = \frac{4 \sin^2 \delta_0(W)}{a_p^2 (W^2 - 4M^2)} = \left\{ 1 + \frac{a_p}{4} (a_p + r_p) (W^2 - 4M^2) + \frac{a_p^2 r_p^2}{64} (W^2 - 4M^2)^2 \right\}^{-1} \quad (6)$$

with  $W$  the final–state di–proton invariant mass and  $\lambda(x, y, z) = x^2 + y^2 + z^2 - 2yz - 2xz - 2xy$  the Källén function.  $W_{\text{max}} = \sqrt{4M^2 + 2MT_{\text{lab}}} - m_\pi$  is the kinematical endpoint of the di–proton invariant mass spectrum. Furthermore,  $a_p = (7.8098 \pm 0.0023)$  fm and  $r_p = (2.767 \pm 0.010)$  fm, taken from ref.[22], are the scattering length and effective range parameter for elastic  $pp$ -scattering including electromagnetic effects. Note that we have fixed the normalization of the correction factor  $F_p(W)$  such that in the limit of vanishing scattering length  $a_p$  (i.e. vanishing final–state interaction),  $F_p(W)$  becomes identical to one (in the effective range approximation). Furthermore, the condition  $F_p(2M) = 1$  ensures that there is no final–state interaction effect exactly at threshold, as it must be according to the definition of the threshold amplitude  $\mathcal{A}$  in Eq.(1). In appendix C we give a simple derivation of  $F_p(W)$  in scattering length approximation (i.e. for  $r_p = 0$ ) using effective field theory methods.

With the help of Eqs.(5,6) we are now in the position to extract the values of  $|\mathcal{A}|$  as shown in table 1. We ignore the data point at the lowest energy since that close to threshold a better treatment of the infinite range Coulomb interaction in terms of proton wave functions would be needed. The empirical value of  $\mathcal{A}$  is thus

$$\mathcal{A}^{(\text{exp})} = (2.7 - i 0.3) \text{ fm}^4, \quad (7)$$

anticipating the positive sign of the real part from the calculation in section 3. Since we are mostly interested in achieving a qualitative picture of the underlying production process, we refrain from assigning an uncertainty to this number. This number should be comparable to the one found by Adam et al. [23], who employ essentially the same method to correct for the final–state interaction but use a different (unspecified) normalization of the T–matrix. In Fig.2 we show the resulting total cross sections in comparison to the data of refs.[1, 2] using Eqs.(5,6,7).

$T_{\text{lab}}$ [MeV]	282.2	285	290	295	300.3	308	314	319	325.6
$\sigma_{\text{tot}}$ [ $\mu\text{b}$ ]	0.148	0.56	1.31	2.06	3.07	4.47	5.25	6.18	7.71
$ \mathcal{A} $ [ $\text{fm}^4$ ]	2.42	2.73	2.69	2.64	2.70	2.71	2.64	2.66	2.73

Table 1: Extracted values for the threshold amplitude  $|\mathcal{A}|$  for the proton laboratory kinetic energies  $T_{\text{lab}}$  and cross sections  $\sigma_{\text{tot}}$  of ref.[1].

### 3 Meson–exchange contributions

In this section, we work out a variety of one–boson exchange contributions related to chiral (pion) and non–chiral (vector meson) physics to the amplitude  $\mathcal{A}$ .

#### 3.1 Tree level Goldstone boson contributions

In this and the following paragraph, we consider tree level and one–loop pion exchanges contributing to the  $pp\pi^0$  production process at threshold. Due to the large proton momentum even at threshold,  $|\vec{p}| \simeq \sqrt{Mm_\pi}$ , it is not appropriate to employ the frequently used heavy baryon formalism for the nucleons. Let us demonstrate the failure of the heavy baryon approach for a simple (but generic) example. Consider diagram b) in Fig.3 which involves a propagating nucleon after emission of the real  $\pi^0$ . We show that this nucleon propagator can not be expanded in powers of  $1/M$  in the usual way. Let  $v^\mu = (1, \vec{0})$  be the four–vector which selects the center–of–mass frame. The four–vector of the propagating nucleon is  $Mv + k$  with  $k^\mu = (-m_\pi/2, \vec{p})$  and  $k^2 = -Mm_\pi$ . We start on the left hand side with the correct relativistic result and then perform the usual  $1/M$  expansion of the heavy baryon formalism,

$$-\frac{1}{m_\pi} = \frac{2M}{(Mv + k)^2 - M^2} = \frac{1}{v \cdot k + k^2/2M} = \frac{1}{v \cdot k} \sum_{n=0}^{\infty} \left( \frac{-k^2}{2M v \cdot k} \right)^n = -\frac{2}{m_\pi} \sum_{n=0}^{\infty} (-1)^n. \quad (8)$$

One sees that infinitely many terms of the  $1/M$ –expansion contribute to the same order. The resulting series does not even converge and oscillates between zero and twice the correct answer. The source of this problem is the extreme kinematics of the reaction  $NN \rightarrow NN\pi$  with  $|\vec{p}| \simeq \sqrt{Mm_\pi}$ . In that case the leading order operator  $\mathcal{O}^{(1)} = iv \cdot \partial$  and the next–to–leading order operator  $\mathcal{O}^{(2)} = -\partial \cdot \partial/2M$  lead to the same result, here,  $\pm m_\pi/2$ . The heavy baryon formalism (and therefore also HBChPT) can not cope with external momenta as large as  $|\vec{p}| \simeq \sqrt{Mm_\pi}$ . This problem is merely related to “trivial” kinematics and can be immediately overcome in fully relativistic calculations. In the latter one does not presume that vertices and propagators can be consistently expanded in inverse powers of the large nucleon mass  $M$ . The occurrence of such non–expandable nucleon propagators is generic to  $NN \rightarrow NN\pi$  and they will of course also enter in loop diagrams. In order to treat correctly the kinematics, one has to evaluate the loops relativistically, even though this may spoil the one–to–one correspondence between the loop and small momentum/quark–mass expansion. A consistent power counting scheme for processes  $NN \rightarrow NN\pi$  involving loops of arbitrary high order is not in sight at the moment.

We thus turn to the relativistic description of the chiral pion–nucleon system. Instead of giving the Lagrangian (see e.g. ref.[24]), we mention only the relevant pion–nucleon vertices. The  $\pi NN$ –vertex (and also the  $\eta NN$ –vertex) is of pseudovector type as required by chiral symmetry. The second order isoscalar chiral  $\pi\pi NN$  contact interaction,  $\pi^0(q_1) + N(p_1) \rightarrow \pi^0(q_2) + N(p_2)$  reads,

$$\frac{i}{f_\pi^2} \left\{ -4c_1 m_\pi^2 + 2c_3 q_1 \cdot q_2 + \frac{c_2'}{2M} [(p_1 + p_2) \cdot q_1 \not{q}_2 + (p_1 + p_2) \cdot q_2 \not{q}_1] + \frac{c_2''}{2M^2} (p_1 + p_2) \cdot q_1 (p_1 + p_2) \cdot q_2 \right\}. \quad (9)$$

This form is unique since on mass–shell it gives the most general second order ( $s \leftrightarrow u$ ) crossing symmetric polynomial contribution to the invariant isoscalar  $\pi N$  amplitudes,

$$A^+(s, u) = \frac{1}{f_\pi^2} \left\{ -4c_1 m_\pi^2 + c_3(s + u - 2M^2) + \frac{c_2''}{8M^2} (s - u)^2 \right\}, \quad B^+(s, u) = \frac{c_2'}{2M f_\pi^2} (s - u), \quad (10)$$

with  $s$  and  $u$  the usual Mandelstam variables. The low–energy constants  $c_1, c_2', c_2'', c_3$  have already been determined (at tree level) in [18] from low–energy  $\pi N$  data and we list their values for completeness:

$$c_1 = -0.64, \quad c_2' = -5.63, \quad c_2'' = 7.41, \quad c_3 = -3.90, \quad (11)$$

all given in  $\text{GeV}^{-1}$ . As it was shown in ref. [25], the numerical values of most of these low–energy constants ( $c_2', c_2'', c_3$ ) can be understood largely from intermediate  $\Delta$  excitations.

Consider first one–pion ( $\pi^0$ ) exchange. The respective diagrams are shown in Figs. 3a,b (with  $\mathcal{M} = \pi^0$ ). We stress that these are relativistic Feynman graphs, i.e. in the intermediate states they contain the full relativistic fermion propagator which sums up several time–orderings. We also note that the graphs with the pion exchange after the emission of the  $\pi^0$  from one of the proton lines does not belong to the final state–interaction according to our treatment (as an on–shell NN–process). We find

$$\mathcal{A}^{(\pi, \text{dir})} = \frac{g_{\pi N}^3}{4M^4(1 + \mu)(2 + \mu)} = 0.48 \text{ fm}^4, \quad (12)$$

with  $g_{\pi N} = 13.4$  the strong pion–nucleon coupling constant. We remark that it is often claimed that the  $pp\pi^0$  final–state should be suppressed due to chiral symmetry. This argument is based on the assumption of the exchanged pion being soft, which, however, is not the case. The  $\pi^0 p$  amplitude with one  $\pi^0$  off its mass–shell is only of linear order in the pion mass  $m_\pi$  (since  $k^2 = -Mm_\pi$ ) and this factor of  $m_\pi$  is cancelled by the pion propagator  $[m_\pi(M + m_\pi)]^{-1}$ . Consequently, as Eq.(12) shows, the threshold amplitude  $\mathcal{A}$  in  $1\pi$ –exchange approximation does not vanish in the chiral limit as it is often claimed. In fact, chiral symmetry does not distinguish the  $pp \rightarrow pp\pi^0$  process from the other  $NN \rightarrow NN\pi$  channels. Next, there is the so–called  $\pi^0$  rescattering, as shown in Fig. 3c,

$$\mathcal{A}^{(\pi, \text{res})} = \frac{g_{\pi N} \mu}{f_\pi^2 M(1 + \mu)} \left[ \frac{c_3}{2} + \left(1 + \frac{\mu}{4}\right) c_2' + \left(1 + \frac{\mu}{4}\right)^2 c_2'' - 2c_1 \right] = 0.46 \text{ fm}^4, \quad (13)$$

with  $f_\pi = 92.4 \text{ MeV}$  the pion decay constant. Again, there is a marked difference to the heavy baryon case. To leading order, the relativistic couplings  $c_2', c_2''$  combine to give the  $c_2 = c_2' + c_2''$  term in the heavy baryon approach. In previous HBChPT calculations the  $c_2$  term was found

with an incorrect prefactor  $1/2$ . The relative factor of two in the relativistic calculation comes from the fact that products of nucleon and pion four-momenta are not dominated anymore by the term nucleon mass times pion energy. For the reaction  $NN \rightarrow NN\pi$  the product of the nucleon and pion three-momenta can be equally large, since  $|\vec{p}| \simeq \sqrt{Mm_\pi}$ .

Interestingly, the combination of low-energy constants in Eq.(13) is dominated (to about 90%) by the last term  $\sim -2c_1$ , which is related to the so-called pion-nucleon sigma-term,  $\sigma_{\pi N}(0) = -4c_1 m_\pi^2$  (to leading order). Therefore the strength of the  $\pi^0$ -rescattering (at threshold) is almost entirely due to this particular chiral symmetry breaking term. The effects from the  $\Delta(1232)$ -resonance encoded in the low-energy constants  $c'_2, c''_2, c_3$  turn out to be very small. In order to check this interpretation, we have evaluated the contributions from explicit  $\Delta(1232)$ -excitations, using the Rarita-Schwinger formalism and the well-satisfied coupling constant relation  $g_{\pi N \Delta} = 3g_{\pi N}/\sqrt{2}$ . We find:

$$\mathcal{A}^{(\Delta)} = \frac{g_{\pi N}^3 \mu}{16M_\Delta^2 M^3 (1 + \mu)} \left\{ \frac{M^2(4 + \mu)(M_\Delta + M(1 - \mu))}{M_\Delta^2 + M^2(2\mu - 1)} + (2Z - 1) \left[ 4(1 + Z)M_\Delta - M(2Z(3 + \mu) + 1 + \mu) \right] \right\} = 0.04 \text{ fm}^4, \quad (14)$$

where we used for the off-shell parameter  $Z = -0.3$ , the value which maximizes the  $\Delta(1232)$ -contribution to the  $P_{33} \pi N$  scattering volume. Such a value of  $Z$  is also consistent with neutral pion photoproduction off protons. The small value of  $\mathcal{A}^{(\Delta)}$  confirms the interpretation of the rescattering contribution Eq.(13) given above.

The next Goldstone boson which can contribute is the  $\eta(547)$ . Consider the graphs in Figs. 3a,b with  $\mathcal{M} = \eta$ . We find

$$\mathcal{A}^{(\eta)} = \frac{g_{\pi N} g_{\eta N}^2 \mu}{4M^2(m_\eta^2 + M^2\mu)(2 + \mu)} = 0.02 \text{ fm}^4, \quad (15)$$

where we have employed the SU(3) value for the  $\eta N$  coupling constant together with the simplified ratio of the octet axial vector coupling constants  $D/F = 1.5$ , which leads to  $g_{\eta N} = 4.6$ . Since this contribution is tiny, the precise value of this coupling does not matter.

### 3.2 Pion loop effects

We do not attempt a full one-loop calculation here, but rather consider certain (simple) classes of loop graphs which are genuine to the process under consideration. We use dimensional regularization and minimal subtraction to eliminate divergences and set the renormalization scale equal to the proton mass  $M$ . For estimating the genuine size of pion loop effect, such a procedure ignoring renormalization via counterterms should be sufficient and the resulting numbers should be considered indicative.

Consider first a certain class of pion loop diagrams which involve the  $\pi\pi$  interaction, compare Fig. 4. Notice that only the full class of diagrams is independent of the choice of the interpolating pion field. Within the calculational scheme mentioned above, this class of graphs gives

$$\mathcal{A}^{(\text{loop},1)} = \frac{g_{\pi N}^3(2 + \mu)(1 - \mu)}{(8\pi M f_\pi)^2(1 + \mu)} \left\{ \ln \mu - \frac{1}{2} + \sqrt{1 + 4\mu} \ln \frac{1 + \sqrt{1 + 4\mu}}{2\sqrt{\mu}} + \int_0^1 dx \int_0^x dy \frac{y}{y^2 + \mu^2(1 - y) + \mu(1 - x)(x - y)} \right\} = -0.10 \text{ fm}^4. \quad (16)$$

We remark that the expression in the curly brackets is not singular in the chiral limit  $\mu \rightarrow 0$ . It has the following  $\mu$ -expansion:  $-1/2 + \sqrt{\mu} \pi^2/8 + \mathcal{O}(\mu \ln \mu)$ . Again, one faces here the usual problem of relativistic loops.  $\mathcal{A}^{(\text{loop},1)}$  does not vanish in the chiral limit  $\mu \rightarrow 0$  and is therefore not suppressed by powers of the pion mass  $m_\pi$  compared to tree graphs. Nevertheless, its numerical value is small. The threshold amplitude  $\mathcal{A}^{(\text{loop},1)}$  is actually proportional to the relativistic loop contribution [24] to the nucleon scalar form factor evaluated at an invariant momentum transfer squared  $t = -Mm_\pi$ ,

$$\mathcal{A}^{(\text{loop},1)} = \frac{g_{\pi N}(2 + \mu)(\mu - 1)}{12Mf_\pi^2 m_\pi^2(1 + \mu)} \sigma_{\pi N}(-M^2\mu)_{\text{loop}} . \quad (17)$$

Whereas ref.[16] claimed that these loop graphs were sizeable and are essential for a quantitative description of the data, we find that they give only a small  $-4\%$  correction compared to the empirical value of  $\mathcal{A}$ . The reason for this discrepancy is to be found in the inappropriate application of the heavy baryon formalism to  $pp \rightarrow pp\pi^0$  in ref.[16]. Next, we consider the entire class of loop graphs proportional to  $g_{\pi N}/f_\pi^4$ , see graphs in Fig.5 and Fig.6. Figs.5 (a) and (b) represent  $\pi^+\pi^-$  exchange between protons (in form of a bubble diagram) before or after the emission of the neutral pion. We find:

$$\begin{aligned} \mathcal{A}^{(\text{loop},2)} &= \frac{g_{\pi N}(2 - \mu)\mu}{768\pi^2 f_\pi^4(2 + \mu)} \left\{ (1 + 6\mu) \ln \mu - \frac{5}{6} - 4\mu + (1 + 4\mu)^{3/2} \ln \frac{1 + \sqrt{1 + 4\mu}}{2\sqrt{\mu}} \right\} \\ &= -0.01 \text{ fm}^4 . \end{aligned} \quad (18)$$

Note that these loop corrections vanish in the chiral limit  $\mu \rightarrow 0$ . In the class of diagrams proportional to  $g_{\pi N}/f_\pi^4$  there is also  $\pi^0$ -exchange between the protons with  $\pi^+$  rescattering on one of the nucleons, see (c) and (d) in Fig.5. These graphs give

$$\begin{aligned} \mathcal{A}^{(\text{loop},3)} &= \frac{g_{\pi N} \mu}{[8\pi f_\pi^2(1 + \mu)(1 - 2\mu)]^2} \left\{ (1 + \mu)(1 - 2\mu)(4 - 6\mu - \mu^2) + (11 - 16\mu + \mu^2 + \mu^3) \right. \\ &\quad \left. \cdot \mu^2 \ln \mu + \mu(1 + \mu)(2 - 2\mu - \mu^2) \sqrt{\mu(4 + \mu)} \ln \frac{2 + \mu + \sqrt{\mu(4 + \mu)}}{2} \right\} \\ &= 0.22 \text{ fm}^4 . \end{aligned} \quad (19)$$

This contribution vanishes again in the chiral limit  $\mu \rightarrow 0$ . Finally, there are graphs where a  $\pi^+\pi^-$ -pair is emitted from one proton and the  $\pi^0$  emission proceeds via charge exchange from the other nucleon line, see Fig.6. Straightforward evaluation of these diagrams gives

$$\begin{aligned} \mathcal{A}^{(\text{loop},4)} &= \frac{g_{\pi N} \mu}{(8\pi f_\pi^2)^2} \left\{ \frac{\mu(9\mu - 2 - \mu^2)}{2(1 + \mu)(1 - 2\mu)} + \frac{6 - 12\mu + 19\mu^2 + 2\mu^3 + \mu^4}{2(1 + \mu)^2(1 - 2\mu)^2} \mu^2 \ln \mu \right. \\ &\quad \left. + \frac{\mu^2(2 - \mu)}{2(1 - 2\mu)^2} \sqrt{\mu(4 + \mu)} \ln \frac{2 + \mu + \sqrt{\mu(4 + \mu)}}{2} + \int_0^1 dx \int_0^x dy y \times \right. \\ &\quad \left. \left[ \frac{2x - 2 - 5y + \mu(3 - 3x - y) + \mu^2(3 - x)}{y^2 + \mu(1 - x)(x - 3y) + \mu^2(1 - 2y + xy)} + \frac{2 - 2x - 3y + \mu(x - 1) + \mu^2}{y^2 + \mu(1 - x)(x + y) + \mu^2(1 - y)} \right] \right\} \\ &= -0.25 \text{ fm}^4 , \end{aligned} \quad (20)$$

a contribution which again vanishes in the chiral limit. Summing all these various loop contributions in Eqs.(16,18,19,20), we find

$$\mathcal{A}^{(\text{loop})} = -0.14 \text{ fm}^4 , \quad (21)$$

which is a rather small number as compared to the tree level pion exchange or the vector meson contributions (section 3.3). We observe sizeable cancelations between the various classes of loop graphs and conclude therefore that these do not play a significant role for explaining the threshold amplitude  $\mathcal{A}$ . The imaginary part of  $\mathcal{A}$  is discussed in appendix B.

### 3.3 Heavy meson exchanges

Due to the large momenta involved, one expects additional contributions due to the exchange of heavier mesons, which are of much shorter range than the pion exchange considered so far. From the symmetry point of view such terms are much less constrained and thus exhibit a certain unavoidable model-dependence. Nevertheless, these terms can play a significant role as first stressed by Lee and Riska [7] and confirmed by Horowitz et al. [8]. We do not discuss here additional effects from vector meson nucleon form factors, which are a model-dependent (and unobservable) concept to account for the finite size of the hadrons involved. Note also that in a strict field-theoretical sense such form factors can not be uniquely defined. At the invariant momentum transfer  $t = -0.127 \text{ GeV}^2$  the form factor effect is not expected to be large. For example, one expects a 10% effect for typical monopole form factors with cut-offs  $\Lambda_{\omega,\rho} \simeq 1.5 \text{ GeV}$ .

Consider first neutral vector mesons. We start with the  $\omega(782)$ . There is sizeable uncertainty about its coupling constant to the nucleon, extreme values are e.g. found in the dispersion-theoretical analysis of the nucleons electromagnetic form factors,  $g_{\omega N} \simeq 21$  [27]. However, it is not clear how one has to transcribe such a value to the one-boson exchange picture of the NN force. In conventional boson-exchange models, the inclusion of the correlated  $\pi\rho$  continuum allows one to work with a coupling constant that is compatible with the SU(3) value,  $g_{\omega N} \simeq 9$  or the value  $g_{\omega N} = 10.1 \pm 0.9$  found from forward NN-dispersion relations [28]. For a detailed discussion, see e.g. ref. [29]. There is agreement that the tensor-to-vector coupling ratio of the  $\omega$ -meson is very small. If we set  $\kappa_\omega = 0$  and use the coupling constant  $g_{\omega N} = 10$ , we get

$$\mathcal{A}^{(\omega)} = \frac{g_{\pi N} g_{\omega N}^2 (2 - \mu)}{2M^2 (M_\omega^2 + M^2 \mu) (2 + \mu)} = 1.35 \text{ fm}^4, \quad (22)$$

which is quite sizeable. In a similar fashion, we evaluate the  $\rho(770)$  contribution. Here, there is less debate about the coupling constant  $g_{\rho N}$  and also, it is well established that the tensor-to-vector coupling ratio  $\kappa_\rho$  is large. For simplicity, we use  $g_{\rho N} = 3$  (obtained from  $\rho$ -universality,  $g_{\rho N} = g_\rho/2$  with  $g_\rho = 6$ ) and  $\kappa_\rho = 6$ . That leads to

$$\mathcal{A}^{(\rho)} = \frac{g_{\pi N} g_{\rho N}^2}{2M^2 (M_\rho^2 + M^2 \mu) (2 + \mu)} \left[ 2 + \mu (\kappa_\rho^2 - \kappa_\rho - 1) + \mu^2 \kappa_\rho \left( 1 + \frac{9}{8} \kappa_\rho \right) \right] = 0.48 \text{ fm}^4. \quad (23)$$

We note that this form is very different from what has been used in the literature so far, where one finds the  $\omega, \rho$ -exchange to be proportional to  $\mu(1 + \kappa_{\omega,\rho})$ . We do not employ any inappropriate non-relativistic approximation here and thus obtain the results shown in Eqs.(22,23). Note that due to the large tensor-to-vector coupling ratio of the  $\rho$ -meson  $\kappa_\rho = 6$  the terms proportional to  $\mu$  and  $\mu^2$  in the square bracket of Eq.(23) are most important. We have also investigated the role of  $\phi(1020)$  exchange, which can be related to the strangeness content of the nucleon wave function. The values of the  $\phi N$  coupling constant span a large range, as documented in table 2 of ref.[30]. To get a more precise number, we proceed as follows. We assume that the tensor-to-vector coupling ratios are given by the dispersive analysis of the nucleon electromagnetic form factors,  $\kappa_\rho = 6.1$ ,  $\kappa_\omega = -0.16$  and  $\kappa_\phi = -0.22$  [27]. Using furthermore the SU(3) relation  $g_{\omega N} = 3g_{\rho N} - \sqrt{2}g_{\phi N}$  [29] together with  $g_{\rho N} = 2.63$  [31] and  $g_{\omega N} = 10.1$  [28], we have  $g_{\phi N} = -1.56$ . This leads to  $\mathcal{A}^{(V)} = \mathcal{A}^{(\rho)} + \mathcal{A}^{(\omega)} + \mathcal{A}^{(\phi)} = (0.38 + 1.40 + 0.02) \text{ fm}^4 = 1.80 \text{ fm}^4$ , which is practically identical to the result obtained above using the simplified coupling constants. Thus, the sum of the vector meson contributions is fairly stable against parameter

variations and also the  $\phi(1020)$  does not play any role. Finally, we remark that substituting  $(g_{\rho N}, M_\rho, \kappa_\rho)$  by  $(e, 0, \kappa_p)$  one can convince oneself that the one-photon exchange gives a tiny correction of  $\mathcal{A}^{(\gamma)} = 0.0085 \text{ fm}^4$ , as it is of course expected.

Another mechanism, first proposed in this context in [13], is the emission of the neutral pion from the anomalous  $\omega\rho\pi$ -vertex, with the  $\rho(770)$  coupling to one and the  $\omega(782)$  to the other proton. This type of graph is similar to well-known meson-exchange currents in electromagnetic processes. The pertinent interaction vertex, with its strength given by the coupling constant  $G_{\omega\rho\pi}$ , can be determined from the anomalous Wess-Zumino-Witten term for vector mesons (we only show the part of relevance here),

$$\mathcal{L}_{\omega\rho\pi} = -\frac{G_{\omega\rho\pi}}{f_\pi} \epsilon^{\mu\nu\alpha\beta} (\partial_\mu \omega_\nu) \vec{\rho}_\alpha \cdot \partial_\beta \vec{\pi} , \quad (24)$$

with  $\epsilon^{\mu\nu\alpha\beta}$  the totally antisymmetric tensor in four dimensions ( $\epsilon^{0123} = -1$ ). Using again the universal  $\rho$ -coupling,  $g_\rho = 6$ , the gauged Wess-Zumino-Witten term for vector mesons leads to the coupling constant

$$G_{\omega\rho\pi} = \frac{3g_\rho^2}{8\pi^2} = 1.37 . \quad (25)$$

Similar values for  $G_{\omega\rho\pi}$  have been found in refs.[32, 33] from systematic studies of  $\omega(782)$ - and  $\phi(1020)$ -decays. The contribution of the anomalous  $\omega\rho\pi$ -vertex to  $\mathcal{A}$  is given by

$$\mathcal{A}^{(\omega\rho\pi)} = \frac{g_{\omega N} g_{\rho N} (1 + \kappa_\rho) G_{\omega\rho\pi} M \mu^2}{2f_\pi (M_\omega^2 + M^2 \mu) (M_\rho^2 + M^2 \mu)} = 0.09 \text{ fm}^4 , \quad (26)$$

which is at first glance quite small. However, due to the two derivatives appearing in Eq.(24), one expects this contribution to be of much larger importance in the P-wave amplitudes. An analogous short range mechanism is the  $\pi^0$  emission from the  $a_0\eta\pi$ -vertex, proposed in ref.[13]. We have evaluated the respective contribution to  $\mathcal{A}$  and found that it is negligibly small,  $\mathcal{A}^{(a_0\eta\pi)} = 0.003 \text{ fm}^4$ . Finally, we do not consider a scalar meson exchange here. First, there is no scalar meson resonance which couples strongly to the nucleon and secondly, the fictitious “ $\sigma(550)$ ” of one-boson exchange models just simulates the long and intermediate range part of uncorrelated  $2\pi$ -exchange in the NN interaction [34]. The latter comes along with pion loops and is to some extent contained in the loop graphs considered above.

### 3.4 Total threshold amplitude

We are now in the position to evaluate the full amplitude  $\mathcal{A}$  from the various contributions. Combining Eqs.(12,13,15,21,22,23,26), we get

$$\begin{aligned} \mathcal{A}^{(\text{thy})} &= \mathcal{A}^{(\pi, \text{dir})} + \mathcal{A}^{(\pi, \text{res})} + \mathcal{A}^{(\eta)} + \mathcal{A}^{(\text{loop})} + \mathcal{A}^{(\omega)} + \mathcal{A}^{(\rho)} + \mathcal{A}^{(\omega\rho\pi)} \\ &= (0.48 + 0.46 + 0.02 - 0.14 + 1.35 + 0.48 + 0.09) \text{ fm}^4 \\ &= 2.74 \text{ fm}^4 , \end{aligned} \quad (27)$$

which compares well with the empirical value given in Eq.(7). The resulting total cross section  $\sigma_{\text{tot}}(T_{\text{lab}})$  is shown in Fig. 2 by the dashed-dotted line. Of course, taken the uncertainty in certain coupling constants and our simplified treatment of the final-state interaction, the 1% agreement between our theoretical prediction for  $\mathcal{A}$  and its empirical value, Eq.(7), should not be taken too serious. We only want to make the point that these well-known boson-exchange diagrams, when evaluated fully relativistically, can explain the near threshold data for  $pp \rightarrow pp\pi^0$ . Note also that the contribution from explicit  $\Delta(1232)$ -excitation, cf. Eq.(14), is contained in the  $\pi^0$  rescattering term via the low-energy constants  $c_2, c_2', c_3$ .

## 4 Charged pion production in $pp$ -collisions

In this section we will discuss charged pion production using the same approach. The T-matrix for charged pion production in proton-proton collisions,  $p_1(\vec{p}) + p_2(-\vec{p}) \rightarrow p + n + \pi^+$ , at threshold in the center-of-mass frame reads (see also appendix A for the general  $NN \rightarrow NN\pi$  threshold T-matrix),

$$T_{\text{th}}^{\text{cm}}(pp \rightarrow pn\pi^+) = \frac{\mathcal{A}}{\sqrt{2}} (i\vec{\sigma}_1 - i\vec{\sigma}_2 + \vec{\sigma}_1 \times \vec{\sigma}_2) \cdot \vec{p} - \sqrt{2}\mathcal{B} i(\vec{\sigma}_1 + \vec{\sigma}_2) \cdot \vec{p}. \quad (28)$$

As indicated by the ordering of the three particles  $pn\pi^+$  in the final state, the spin-operator  $\vec{\sigma}_1$  is understood to be sandwiched between the spin-states of the ingoing proton  $p_1(\vec{p})$  and those of the outgoing proton, while  $\vec{\sigma}_2$  acts between the proton  $p_2(-\vec{p})$  and the outgoing neutron. Since the  $pn$ -system at rest can be in a spin-singlet or in a spin-triplet state two different transitions are possible at threshold. The threshold amplitude for the singlet transition  ${}^3P_0 \rightarrow {}^1S_0s$  is by isospin symmetry proportional (with a factor  $1/\sqrt{2}$ ) to the threshold amplitude  $\mathcal{A}$  for the reaction  $pp \rightarrow pp\pi^0$  introduced in Eq.(1). The new threshold amplitude for the triplet transition  ${}^3P_1 \rightarrow {}^3S_1s$  is called  $\mathcal{B}$  and the factor  $-\sqrt{2}$  was taken out for convenience in Eq.(28). In analogy to Eq.(3) one deduces from unitarity

$$\mathcal{B} = |\mathcal{B}| e^{i\delta({}^3P_1)}, \quad (29)$$

with the  ${}^3P_1$   $pp$  phase shift to be taken at  $T_{\text{lab}}^{\text{th}} = 292.3$  MeV, where  $\delta({}^3P_1) = -28.1^\circ$  (FA95 solution of VPI). Because of this larger phase fixed by unitarity the imaginary part  $\text{Im}\mathcal{B}$  will contribute non-negligibly to the total cross sections near threshold. Notice, that the abovementioned unitarity relation Eq.(29) neglects the (small) inelasticity due to the  $pp \rightarrow d\pi^+$  channel which opens 4.8 MeV lower at  $T_{\text{lab}} = 287.5$  MeV.

### 4.1 Extraction of the threshold amplitudes

Employing the same method as in section 2.2 to correct for the strong S-wave  $pn$  final-state interaction, the unpolarized total cross section for  $pp \rightarrow pn\pi^+$  reads,

$$\begin{aligned} \sigma_{\text{tot}}(T_{\text{lab}}) &= \left(\frac{M}{4\pi}\right)^3 \frac{2\sqrt{T_{\text{lab}}}}{(2M + T_{\text{lab}})^{3/2}} \\ &\times \int_{M+M_n}^{W_{\text{max}}} \frac{dW}{W} \sqrt{\lambda(W^2, M^2, M_n^2) \lambda(W^2, m_{\pi^+}^2, 4M^2 + 2MT_{\text{lab}})} \\ &\times \left\{ |\mathcal{A}|^2 F_s(W) + 2|\mathcal{B}|^2 F_t(W) \right\}. \end{aligned} \quad (30)$$

The correction factors from the  $pn$  singlet and triplet S-wave final state interaction are given in the effective range approximation by

$$F_{s,t}(W) = \left\{ 1 + a_{s,t}(a_{s,t} + r_{s,t})P_*^2 + \frac{1}{4}a_{s,t}^2 r_{s,t}^2 P_*^4 \right\}^{-1}, \quad (31)$$

with  $W$  the final-state proton-neutron invariant mass and  $W_{\text{max}} = \sqrt{4M^2 + 2MT_{\text{lab}}} - m_{\pi^+}$ .  $M$  still denotes the proton mass and  $M_n = 939.57$  MeV stands for the neutron mass. The quantity  $P_*^2 = \lambda(W^2, M^2, M_n^2)/4W^2$  is the squared  $pn$  center-of-mass momentum. The singlet

and triplet scattering lengths and effective range parameters for elastic  $np$ -scattering are taken from [22], their empirical values being  $a_s = (23.748 \pm 0.010)$  fm,  $a_t = (-5.424 \pm 0.004)$  fm,  $r_s = (2.75 \pm 0.05)$  fm and  $r_t = (1.759 \pm 0.005)$  fm. We neglect here the coupling between the  ${}^3S_1$  and the  ${}^3D_1$   $pn$ -states, which should be very small at the energies under consideration. Such effects go beyond the accuracy of the effective range approximation and our treatment of the  $pn$  final-state interaction.

The data base of total cross sections for the process  $pp \rightarrow pn\pi^+$  in the 30 MeV region above threshold consists at present of five data points measured at IUCF [4]. We leave out the data point at the highest energy  $T_{\text{lab}} = 319.2$  MeV where the  $\pi^+$  angular distributions are no more isotropic and thus P-waves start to become important. We also found it important to ignore the data point at the lowest energy  $T_{\text{lab}} = 294.3$  MeV. Using Eq.(30) for the total cross section and the value of  $|\mathcal{A}| = 2.72$  fm<sup>4</sup> as determined from the  $pp \rightarrow pp\pi^0$  data, one finds in a least square fit of the remaining three data points for the modulus of the triplet threshold amplitude,

$$|\mathcal{B}| = 3.16 \text{ fm}^4, \quad (32)$$

with a very small total  $\chi^2 = 0.044$ . For these values of  $|\mathcal{A}|$  and  $|\mathcal{B}|$  the data point at  $T_{\text{lab}} = 319.2$  MeV is underestimated by 17% in the S-wave approximation (see table 2). An unconstrained fit of the same three data points gives  $|\mathcal{A}| = 3.00$  fm<sup>4</sup> and  $|\mathcal{B}| = 3.15$  fm<sup>4</sup> with a marginally smaller total  $\chi^2 = 0.042$ . It is quite remarkable that  $|\mathcal{A}|$  is found to be in 10% agreement with the value obtained from fitting the many precise near threshold  $pp \rightarrow pp\pi^0$  data. Due to the very strong  $pn$  final-state interaction in the  ${}^1S_0$  exit channel ( $a_s = 23.75$  fm) the singlet transition contributes a factor 30 to 40 less to the total cross section than the triplet transition. From our fit we get at the lowest energy  $T_{\text{lab}} = 294.3$  MeV a total cross section of  $0.57 \mu\text{b}$ , compared to the experimental value of  $(0.71 \pm 0.04) \mu\text{b}$  given in ref.[4]. Only if one widens the error band of this data point by the  $\pm 15\%$  absolute normalization uncertainty it becomes (at the lower end) marginally consistent with the remaining data. If, however, the data point at  $T_{\text{lab}} = 294.3$  MeV were included in an unconstrained fit, very different values of the threshold amplitudes,  $|\mathcal{A}| = 6.76$  fm<sup>4</sup> and  $|\mathcal{B}| = 2.91$  fm<sup>4</sup>, would be found with a total  $\chi^2 = 1.0$ . In particular  $|\mathcal{A}|$  would be a factor 2.5 larger than the one obtained from the fit to the  $pp \rightarrow pp\pi^0$  data. Of course, such a large deviation from isospin symmetry is unacceptable.

$T_{\text{lab}}$ [MeV]	294.3	295.1*	298.0*	299.3	306.3	314.1	319.2
$\sigma_{\text{tot}}^{\text{exp}}$ [ $\mu\text{b}$ ]	0.71	1.1*	3.84*	4.81	13.91	25.5	41.1
$\delta\sigma_{\text{tot}}^{\text{exp}}$ [ $\mu\text{b}$ ]	$\pm 0.04$	$\pm 0.3^*$	$\pm 0.37^*$	$\pm 0.24$	$\pm 0.65$	$\pm 1.6$	$\pm 1.7$
$\sigma_{\text{tot}}^{\text{fit}}$ [ $\mu\text{b}$ ]	0.57	1.07	3.46	4.81	13.82	25.76	34.14

Table 2: Total cross sections for  $pp \rightarrow pn\pi^+$  as a function of  $T_{\text{lab}}$ . The data are taken from ref.[4] and the preliminary data points from COSY-TOF [35] are marked by an asterik. The (constrained) fit is described in the text.

Anticipating the positive sign of the real part from the calculation in the following section and using the information from the  ${}^3P_1$  phase shift, one gets the following experimental value of the triplet threshold amplitude  $\mathcal{B}$ ,

$$\mathcal{B}^{(\text{exp})} = (2.8 - i 1.5) \text{ fm}^4. \quad (33)$$

This number should be considered indicative since the systematic error of the extraction method is not under control when only three data points are fitted. Notice also that the imaginary part is fairly sizeable, quite different from  $\mathcal{A}$ , the threshold amplitude for  $pp \rightarrow pp\pi^0$ .

## 4.2 Diagrammatic approach

Next, we turn to the evaluation of the relativistic Feynman diagrams contributing to  $pp \rightarrow pn\pi^+$  at threshold. In addition to the ones considered for  $pp \rightarrow pp\pi^0$ , there is now the possibility for isovector pion–rescattering. The chiral  $\pi N$  Lagrangian contains such vertices at leading order (the so–called Weinberg–Tomozawa vertex) and at next–to–leading order (a vertex proportional to the low–energy constant  $c_4 = 2.25 \text{ GeV}^{-1}$ ). In fact there are always two isovector rescattering diagrams, one with a  $\pi^0$  and another one with a  $\pi^+$  being exchanged between the nucleons. The isospin factors of both diagrams are equal with opposite sign. However, before adding them one has to account for the fact that the role of  $p$  and  $n$  is interchanged in both graphs. This is done by multiplying those graphs where the final state neutron  $n$  comes from the initial state proton  $p_1(\vec{p})$  with the negative spin–exchange operator  $-(1 + \vec{\sigma}_1 \cdot \vec{\sigma}_2)/2$ . Altogether, one finds from isovector pion–rescattering at leading and next–to–leading order,

$$\mathcal{B}^{(\pi,\text{iv})} = \frac{g_{\pi N}(c_4 m_\pi - 1)}{2M^2 f_\pi^2 (1 + \mu)} = -0.82 \text{ fm}^4 . \quad (34)$$

Of course, we neglect here the small isospin breaking due the different charged and neutral pion masses and the different proton and neutron masses. From the other pseudoscalar meson ( $\pi$  and  $\eta$ ) exchange diagrams, one finds the following contributions to the triplet amplitude,

$$\mathcal{B}^{(\pi,\text{dir})} = \frac{g_{\pi N}^3 (3 + 2\mu)}{4M^4 (1 + \mu)(2 + \mu)} = 1.58 \text{ fm}^4 , \quad (35)$$

$$\mathcal{B}^{(\pi,\text{res})} = \mathcal{A}^{(\pi,\text{res})} = 0.46 \text{ fm}^4 , \quad (36)$$

$$\mathcal{B}^{(\eta)} = -\mathcal{A}^{(\eta)} = -0.02 \text{ fm}^4 , \quad (37)$$

(see also Eqs.(13,15)). Note that the (direct)  $1\pi$ –exchange contribution  $\mathcal{B}^{(\pi,\text{dir})}$  is rather large due to an enhancement factor  $3+2\mu$  in comparison to  $\mathcal{A}^{(\pi,\text{dir})}$  given in Eq.(12). The dominance of the chiral one–pion exchange in the triplet transition  ${}^3P_1 \rightarrow {}^3S_1$  found here supports the argument of [15] concerning the dominant role of the long range (chiral) pion exchange in the reaction  $pp \rightarrow d\pi^+$  which proceeds via the same transition near threshold.

From the vector meson ( $\rho$  and  $\omega$ ) exchange diagrams one finds the following contributions to  $\mathcal{B}$ ,

$$\mathcal{B}^{(\omega)} = \frac{g_{\pi N} g_{\omega N}^2}{M^2 (M_\omega^2 + M^2 \mu)(2 + \mu)} = 1.46 \text{ fm}^4 , \quad (38)$$

$$\mathcal{B}^{(\rho)} = \frac{g_{\pi N} g_{\rho N}^2 (\mu \kappa_\rho - 4)}{4M^2 (M_\rho^2 + M^2 \mu)(2 + \mu)} \left[ 3 + \mu \left( 2 + \frac{\kappa_\rho}{4} \right) \right] = -0.37 \text{ fm}^4 , \quad (39)$$

$$\mathcal{B}^{(\omega\rho\pi)} = 0 . \quad (40)$$

One observes that the sizeable  $\omega$ –exchange contribution  $\mathcal{B}^{(\omega)}$  is approximately equal to  $\mathcal{A}^{(\omega)}$  given in Eq.(22). Note also that the expression for  $\omega$ –exchange cannot be recovered by simply

substituting the vector meson mass and coupling constants in the expression for  $\rho$ -exchange. The reason for that are certain diagrams with (charged)  $\rho^+$ -exchange which have no analogy in the case of the (neutral)  $\omega$ -meson. In the spirit of vector meson dominance one could also think of an isovector  $\pi\rho NN$  contact vertex of the form

$$\mathcal{L}_{\pi\rho N} = \frac{g_\rho g_{\pi N}}{2M} \bar{N} \gamma^\mu \gamma_5 \vec{\tau} \cdot (\vec{\pi} \times \vec{\rho}_\mu) N . \quad (41)$$

The form of this vertex and the coupling constant in front are copied from the Kroll–Ruderman term for charged pion photoproduction replacing the charge  $e$  by the universal  $\rho$ -coupling  $g_\rho = 6$  and the photon field by the isotriplet  $\rho$ -meson field  $\vec{\rho}_\mu$ . The respective  $\rho^0$  and  $\rho^+$  exchange diagrams give rise to the following contribution to the triplet amplitude,

$$\mathcal{B}^{(\rho, \text{KR})} = \frac{g_{\pi N} g_\rho g_{\rho N}}{M^2 (M_\rho^2 + M^2 \mu)} \left( 1 - \frac{\mu}{4} \kappa_\rho \right) = 0.45 \text{ fm}^4 . \quad (42)$$

Admittedly, this contribution is somewhat speculative since the Kroll–Ruderman vertex for  $\rho$ -mesons presumes a particular realization of vector meson dominance. We do not investigate in further detail pion loop diagrams contributing to  $\mathcal{B}$ , since they will turn out to be small in analogy to the amplitude  $\mathcal{A}$  discussed in section 3.2 (for the classes of diagrams calculated there). The imaginary part of the triplet amplitude  $\mathcal{B}$  can only be generated in one-pion loop approximation by the two-pion exchange box diagrams shown in Fig. 9 and evaluated in appendix B. It can, however, not be expected that the one-pion loop approximation will be sufficiently accurate, since the process  $NN \rightarrow NN\pi$  at threshold is also sensitive to short distance dynamics. This needs further study but goes beyond the scope of this paper. A detailed discussion of the imaginary parts of  $\mathcal{A}$  and  $\mathcal{B}$  in one pion loop approximation is given in appendix B. Summing up the various tree level contributions given in Eqs.(34,35,36,37,38,39,40,42) we get,

$$\mathcal{B}^{(\text{thy})} = 2.74 \text{ fm}^4 , \quad (43)$$

which is very close the real part of the experimental value in Eq.(33),  $\text{Re } \mathcal{B}^{(\text{exp})} = 2.8 \text{ fm}^4$ . We thus conclude that also the real part of the triplet amplitude  $\text{Re } \mathcal{B}$  can be well understood in terms of these well-known tree-level meson exchange diagram when evaluated fully relativistically. Of course, the relatively large imaginary part  $\text{Im } \mathcal{B}^{(\text{exp})} = -1.5 \text{ fm}^4$  (more than half as large as the empirical real part) remains unexplained in tree approximation. As mentioned earlier this imaginary part originates (because of unitarity) from the fact that the  ${}^3P_1$   $pp$  phase shift is rather large at the pion production threshold. The large imaginary part  $\text{Im } \mathcal{B}$  thus reflects the strong initial state interaction in the  ${}^3P_1$  entrance channel. For the singlet transition amplitude  $\mathcal{A}$  the situation is different. Accidentally, the  ${}^3P_0$   $pp$  phase shift is very small at the pion production threshold and thus there is only weak initial state interaction in the  ${}^3P_0$  entrance channel. Another mechanism which could contribute (significantly) to  $\text{Im } \mathcal{B}$  is the two-step process  $pp \rightarrow d\pi^+ \rightarrow pn\pi^+$ . The threshold for the deuteron channel  $pp \rightarrow d\pi^+$  opens 4.8 MeV lower at  $T_{\text{lab}} = 287.5 \text{ MeV}$  and the corresponding total cross sections are more than an order of magnitude larger [3, 4] than the ones for  $pp \rightarrow pn\pi^+$ .

We have done several checks on our treatment of the  $pn$  final-state interaction. First, we compared the effective range approximation with the empirical values of the  ${}^1S_0$  and  ${}^3S_1$   $pn$  phase shifts in the energy range relevant here and found that deviations are smaller than 2%. Secondly, we have studied the  $\pi^+$  production cross section as a function of the  $pn$  invariant

mass  $W$  (given by Eq.(30) without  $dW$ -integration) and found good agreement with the data of [4], cf. Fig.7. From all this we conclude that our treatment of the  $pn$  final-state interaction is fairly realistic.

Finally, we believe that all the features of the processes  $pp \rightarrow pN\pi$  that we have learned here from the relativistic diagrammatic approach presented here will be useful for further studies within more complete dynamical models, which e.g. treat initial- and final-state interactions simultaneously. We also remark that a similar covariant one-boson exchange model has been developed in ref.[36], which describes the data at much higher energies,  $0.3 \text{ GeV} < T_{\text{lab}} < 2.0 \text{ GeV}$ . The same model has been applied to threshold data in ref.[37]. These authors introduce in addition (unobservable) meson nucleon form factors and energy-dependent coupling constants. This makes a direct comparison between their work and ours very difficult. However, no isoscalar pion rescattering and no pion loops are considered. Similar to our finding it is concluded that  $\omega(782)$  exchange is important close to pion production threshold and that the  $\Delta(1232)$  plays no role.

## 5 Eta-meson production in $pp$ -collisions

In this section we will discuss  $\eta$ -production using a similar approach. The T-matrix for  $\eta$ -production in proton-proton collisions,  $p_1(\vec{p}) + p_2(-\vec{p}) \rightarrow p + p + \eta$ , at threshold in the center-of-mass frame reads (see also appendix A),

$$T_{\text{th}}^{\text{cm}}(pp \rightarrow pp\eta) = \mathcal{C} (i\vec{\sigma}_1 - i\vec{\sigma}_2 + \vec{\sigma}_1 \times \vec{\sigma}_2) \cdot \vec{p}. \quad (44)$$

with  $\mathcal{C}$  the (complex) threshold amplitude for  $\eta$ -production. The  $\eta$ -production threshold is reached at a proton laboratory kinetic energy  $T_{\text{lab}}^{\text{th}} = m_\eta(2 + m_\eta/2M) = 1254.6 \text{ MeV}$ , where  $m_\eta = 547.45 \text{ MeV}$  denotes the eta-meson mass.

### 5.1 Extraction of the threshold amplitude

In the case of  $\eta$ -production near threshold it is also important to take into account the  $\eta p$  final-state interaction, since the  $\eta N$ -system interacts rather strongly near threshold. In fact a recent coupled-channel analysis [38] of the  $(\pi N, \eta N)$ -system finds for the real part of the  $\eta N$  scattering length  $\text{Re } a_{\eta N} = (0.717 \pm 0.030) \text{ fm}$ . For comparison, this value is a factor 5.7 larger than the  $\pi^- p$  scattering length,  $a_{\pi^- p} = 0.125 \text{ fm}$  [39], measured in pionic hydrogen.

We assume that the correction due to the S-wave  $\eta p$  final-state interaction near threshold can be treated in effective range approximation analogous to the S-wave  $pp$  final-state interaction. We furthermore make the assumption that the final state interactions in the  $pp$  subsystem and in the two  $\eta p$  subsystems do not influence each other and that they factorize. These are of course very strong assumptions, but as we will see soon, such a simple ansatz for the final-state interaction in the  $pp\eta$  three-body system allows to describe rather accurately the energy dependence of the total cross section  $\sigma_{\text{tot}}(pp \rightarrow pp\eta)$  near threshold. Using the factorization ansatz mentioned before, the unpolarized total cross section for  $pp \rightarrow pp\eta$  reads,

$$\begin{aligned} \sigma_{\text{tot}}(T_{\text{lab}}) &= |\mathcal{C}|^2 \left(\frac{M}{4\pi}\right)^3 \frac{2\sqrt{T_{\text{lab}}}}{(2M + T_{\text{lab}})^{3/2}} \int_{2M}^{W_{\text{max}}} dW W F_p(W) \\ &\times \int_{s_\eta^-}^{s_\eta^+} ds_\eta F_\eta(s_\eta) F_\eta(6M^2 + 2MT_{\text{lab}} + m_\eta^2 - W^2 - s_\eta). \end{aligned} \quad (45)$$

with  $W_{\max} = \sqrt{4M^2 + 2MT_{\text{lab}}} - m_\eta$  the endpoint of the di-proton invariant mass spectrum and  $F_p(W)$  given by Eq.(6). The variable  $s_\eta$  is the invariant mass squared of the first  $\eta p$ -pair and the argument of the last function  $F_\eta(\tilde{s}_\eta)$  in Eq.(45),  $\tilde{s}_\eta = 6M^2 + 2MT_{\text{lab}} + m_\eta^2 - W^2 - s_\eta$ , is the invariant mass squared of the second  $\eta p$ -pair. The expressions

$$s_\eta^\pm = 3M^2 + MT_{\text{lab}} + \frac{1}{2}(m_\eta^2 - W^2) \pm \frac{1}{2W} \sqrt{(W^2 - 4M^2)\lambda(W^2, m_\eta^2, 4M^2 + 2MT_{\text{lab}})} \quad (46)$$

give the boundaries of the  $pp\eta$  three-body phase space in the  $(s_\eta, W^2)$ -plane. Obviously, the formula for the total cross section, Eq.(45), is invariant under the permutation of the two  $\eta p$ -pairs,  $s_\eta \leftrightarrow \tilde{s}_\eta$ , since  $s_\eta^\pm = \tilde{s}_\eta^\mp$ . Furthermore, the correction factor  $F_\eta(s_\eta)$  due to the S-wave  $\eta p$  final-state interaction reads in effective range approximation,

$$F_\eta(s_\eta) = \left| \frac{f_{\eta N}^{0+}(s_\eta)}{a_{\eta N}} \right|^2 = \left| 1 - \frac{i a_{\eta N}}{2\sqrt{s_\eta}} \sqrt{\lambda(s_\eta, m_\eta^2, M^2)} + \frac{a_{\eta N} r_{\eta N}}{8s_\eta} \lambda(s_\eta, m_\eta^2, M^2) \right|^{-2}. \quad (47)$$

Here,  $f_{\eta N}^{0+}(s_\eta)$  is the S-wave  $\eta N$  elastic scattering amplitude. The (complex)  $\eta N$  scattering length  $a_{\eta N} = ((0.717 \pm 0.030) + i(0.263 \pm 0.025))$  fm is taken from ref.[38] and the (complex)  $\eta N$  effective range parameter  $r_{\eta N} = ((-1.50 \pm 0.13) - i(0.24 \pm 0.04))$  fm stems from ref.[40]. It is important to note that both ref.[38] and ref.[40] using quite different methods agree within error bars on the value of the  $\eta N$  scattering length  $a_{\eta N}$ .

Using Eq.(45,46,47) for the total cross section and the central values of  $a_{\eta N}$  and  $r_{\eta N}$  one finds in a least square fit of the six data points from CELSIUS [5] for the modulus of the threshold amplitude

$$|\mathcal{C}| = 1.32 \text{ fm}^4, \quad (48)$$

with a total  $\chi^2 = 3.8$ . The resulting energy dependent cross section from threshold up to  $T_{\text{lab}} = 1375$  MeV is shown in Fig. 8 together with the data from CELSIUS [5].<sup>#2</sup> It is rather astonishing that one can describe the total cross section data up to 100 MeV above threshold with a constant threshold amplitude  $\mathcal{C}$  and a simple factorization ansatz for the three-body final-state interaction.

## 5.2 Diagrammatic approach

Next, we turn to the evaluation of the relativistic Feynman diagrams contributing to  $pp \rightarrow pp\eta$  at threshold. The resulting expressions can essentially be copied from the case  $pp \rightarrow pp\pi^0$  making only the substitution  $(g_{\pi N}, m_\pi) \rightarrow (g_{\eta N}, m_\eta)$ . One finds for  $\pi^0, \eta, \omega, \rho^0$ -exchange

$$\mathcal{C}^{(\pi^0)} = \frac{g_{\eta N} g_{\pi N}^2 m_\eta}{4M^2(m_\pi^2 + Mm_\eta)(2M + m_\eta)} = 0.17 \text{ fm}^4, \quad (49)$$

$$\mathcal{C}^{(\eta, \text{dir})} = \frac{g_{\eta N}^3}{4M^2(M + m_\eta)(2M + m_\eta)} = 0.02 \text{ fm}^4, \quad (50)$$

$$\mathcal{C}^{(\omega)} = \frac{g_{\eta N} g_{\omega N}^2 (2M - m_\eta)}{2M^2(M_\omega^2 + Mm_\eta)(2M + m_\eta)} = 0.23 \text{ fm}^4, \quad (51)$$

$$\begin{aligned} \mathcal{C}^{(\rho^0)} &= \frac{g_{\eta N} g_{\rho N}^2}{2M(M_\rho^2 + Mm_\eta)(2M + m_\eta)} \\ &\times \left[ 2 + \frac{m_\eta}{M} (\kappa_\rho^2 - \kappa_\rho - 1) + \frac{m_\eta^2}{M^2} \kappa_\rho \left( 1 + \frac{9}{8} \kappa_\rho \right) \right] = 0.50 \text{ fm}^4. \end{aligned} \quad (52)$$

<sup>#2</sup>Earlier data from SATURNE [41, 42, 43] do not have the same accuracy and are not considered further.

Note that the  $\rho^0$  exchange has become dominant because of the large tensor-to-vector coupling ratio  $\kappa_\rho = 6$  and the larger ratio  $m_\eta/M = 0.58$ .<sup>#3</sup> Besides these diagrams with  $\eta$ -emission before and after meson exchange between the protons, one has to account for the strong  $\eta p$  rescattering. Microscopically, the strong  $\eta N$  S-wave interaction originates (among other things) from the nucleon resonance  $S_{11}(1535)$  which is supposed to have a very large coupling to the  $\eta N$ -channel. Instead of introducing this resonance together with several parameters (mass, width, coupling constant), we will merely introduce here a local  $NN\eta\eta$  contact vertex of the form

$$\mathcal{L}_{\eta N} = K \bar{N}(x)N(x) \eta^2(x) . \quad (53)$$

The interaction strength  $K$  is then determined by the real part of the  $\eta N$  scattering length. This means that the pseudovector Born graphs plus the contact vertex sum up to give the empirical value of  $\text{Re } a_{\eta N} = 0.717 \text{ fm}$ . This leads to the equation

$$4\pi \left(1 + \frac{m_\eta}{M}\right) \text{Re } a_{\eta N} = 2K - \frac{g_{\eta N}^2 m_\eta^2}{M(4M^2 - m_\eta^2)} , \quad (54)$$

which results in a value of  $K = 7.41 \text{ fm}$ . The  $\eta$ -rescattering graph (analogous to Fig. 3c) leads to the following contribution to the threshold amplitude,

$$\mathcal{C}^{(\eta,\text{res})} = \frac{g_{\eta N} K}{M m_\eta (M + m_\eta)} = 0.40 \text{ fm}^4 . \quad (55)$$

Evidently, all contributions to  $\mathcal{C}$  scale with the (empirically not well determined)  $\eta N$ -coupling constant  $g_{\eta N}$ . The numbers given in Eqs.(45,46,47,48,51) which add up to the empirical value of  $|\mathcal{C}| = 1.32 \text{ fm}^4$  follow with  $g_{\eta N} = 5.3$ . Such a value of  $g_{\eta N}$  is consistent with all existing empirical information on it. The SU(3) flavor symmetry connects the pion-nucleon and eta-nucleon coupling constants via the  $D/F$  ratio (of the baryon octet axial vector couplings),

$$g_{\eta N} = g_{\pi N} \frac{3 - D/F}{\sqrt{3}(1 + D/F)} . \quad (56)$$

Using  $g_{\pi N} = 13.4$ , the for our purpose optimal value  $g_{\eta N} = 5.3$  requires a ratio  $D/F = 1.37$ . In fact a systematic analysis of semileptonic hyperon decays in ref.[45] gives  $D/F = 1.58 \pm 0.07$ , not far from this number. Of course, SU(3) is broken to some extent by the strange quark mass. For a recent update, see e.g. [46]. There is one further contribution we have not discussed so far, related to the  $a_0\eta\pi$ -coupling. This coupling is rather uncertain. If one assumes that the diagrams with  $\eta$ -emission from the  $a_0\eta\pi$ -vertex contribute with a positive sign,

$$\mathcal{C}^{(a_0\eta\pi)} = \frac{g_{a_0 N} g_{\pi N} (c_d m_\eta^2 - 2c_m m_\pi^2)}{\sqrt{6} M f_\pi^2 (M_{a_0}^2 + M m_\eta)(m_\pi^2 + M m_\eta)} = 0.05 \text{ fm}^4 , \quad (57)$$

one can even lower the  $\eta N$ -coupling constant to  $g_{\eta N} = 5.1$ . We used here  $g_{a_0 N} = 4.5$  [47] and  $c_d = 32 \text{ MeV}$ ,  $c_m = 42 \text{ MeV}$  [48]. We also note the one-boson exchange model of [47] for elastic NN-scattering uses an  $\eta N$ -coupling constant of  $g_{\eta N}^{\text{OBE}} = 6.8$  not far from our value  $g_{\eta N} = 5.3$ . The results of our approach applied to the reaction  $pn \rightarrow pn\eta$  are briefly discussed in appendix A.

The main point we want to make here is that even the  $pp \rightarrow pp\eta$  threshold amplitude can be understood in terms of these well-known meson exchange diagrams when evaluated relativistically. With rather mild assumptions on the coupling constant  $g_{\eta N}$  and the form of the  $\eta N$ -rescattering one can easily reproduce the empirical value  $|\mathcal{C}| = 1.32 \text{ fm}^4$ . For another boson-exchange approach to  $\eta$ -production emphasising the role of the  $S_{11}(1535)$  nucleon resonance, see e.g. [49, 50] (and references therein).

<sup>#3</sup>Interestingly, recent measurements of the angular distributions in  $pp \rightarrow pp\eta$  suggest the dominance of vector meson exchange [44].

### 5.3 Comments on $\eta'$ -production near threshold

Finally, we like to comment on the recent  $\eta'$ -production data near threshold from COSY [51] and SATURNE [43]. Taken face value, the energy dependence of the four COSY cross section data points is best described by the pure three-body phase space behavior (as shown by the dotted curve in Fig. 2 of ref.[51]). Of course, it is hard to imagine that the  $pp$  final-state interaction does not play a role for  $pp \rightarrow pp\eta'$  that close to threshold where these data were measured. We have analyzed the combined COSY and SATURNE data (six data points) within our approach including the  $pp$  final-state interaction in effective range approximation. Only if one ignores the COSY data at the two lowest energies (at cm excess energies of 1.5 and 1.7 MeV, respectively), one can fit the remaining four data points with a modulus of the threshold amplitude of  $|\mathcal{C}'| = 0.21 \text{ fm}^4$  with a small total  $\chi^2 = 2.4$ . This fit leads to values of the total cross section at the two lowest energy points of 5.2 nb and 6.3 nb (see also table 3). These numbers are more than twice as large as the corresponding central values given in ref.[51]. Note, however, that in Fig.2 of ref.[51] sizeable uncertainties in the excess energy are given, e.g. the lowest point is at  $Q = (1.5 \pm 0.5) \text{ MeV}$ . Our discussion always refers to the central  $Q$  values.

$Q$ [MeV]	1.5	1.7	2.9	3.7	4.1	8.3
$\sigma_{\text{tot}}^{\text{exp}}$ [nb]	$2.5 \pm 0.5$	$2.9 \pm 1.1$	$12.7 \pm 3.2$	$19.2 \pm 2.7$	$25.2 \pm 3.6$	$43.6 \pm 6.5$
$\sigma_{\text{tot}}^{\text{fit}}$ [nb]	5.23	6.29	13.34	18.45	21.09	50.13

Table 3: Total cross sections for  $pp \rightarrow pp\eta'$  as a function of the cm excess energy  $Q = \sqrt{4M^2 + 2MT_{\text{lab}}} - 2M - M_{\eta'}$  (only the mean value is given). The data are from refs.[43, 51]. The fit is described in the text.

Within the relativistic one-boson ( $\pi^0, \eta, \omega, \rho^0$ ) exchange model the fit value  $|\mathcal{C}'| = 0.21 \text{ fm}^4$  implies the relation  $g_{\eta'N}(1 - 1.28\epsilon) = 1.12$ . Here  $g_{\eta'N}$  denotes the  $\eta'N$ -coupling constant and  $\epsilon$  is the fraction of pseudoscalar  $\eta'NN$ -coupling (since the  $\eta'(958)$  is no Goldstone boson there is no reason to favor the pseudovector coupling). Interestingly, only the tensor interaction of the  $\rho$ -exchange ( $\sim \kappa_\rho$ ) is sensitive to the parameter  $\epsilon$ .

According to ref.[52] one can relate the  $\eta'N$ -coupling constant to the quark helicity contribution to the proton spin,  $\Delta\Sigma = \sqrt{3/2}g_{\eta'N}f_\pi/M + 0.15$ . Using the recent determination  $\Delta\Sigma = 0.45 \pm 0.09$  of ref.[53] from deep inelastic polarized lepton scattering, one can extract within the relativistic one-boson exchange model an  $\eta'N$ -coupling constant of  $g_{\eta'N} = 2.5 \pm 0.7$  and a pseudoscalar coupling fraction of  $\epsilon = 0.4 \pm 0.1$ . It remains to be seen whether other  $\eta'$ -production processes (e.g. photoproduction  $\gamma p \rightarrow \eta'p$ ) are consistent with these values. The exchange of  $\pi^0, \omega$  and  $\rho^0$  contribute to  $|\mathcal{C}'| = 0.21 \text{ fm}^4$  approximately 30%, 20% and 50%, respectively. For another  $1\pi$ -exchange model to  $\eta'$ -production, see e.g. [54].

### Acknowledgements

We thank A. Svarc for information on the  $\eta N$  scattering length. We are particularly grateful to C. Hanhart who pointed out an error concerning the calculation of  $\mathcal{B}$  in the original version of the manuscript.

# A General threshold T–matrices

In this appendix, we write down the general form of the threshold T–matrices for  $NN \rightarrow NN\pi$  and  $NN \rightarrow NN\eta$  using the isospin formalism for the two–nucleon system. In the case of (isovector) pion production one has,

$$\begin{aligned} \text{T}_{\text{th}}^{\text{cm}}(NN \rightarrow NN\pi) &= \frac{\mathcal{A}}{2} (i\vec{\sigma}_1 - i\vec{\sigma}_2 + \vec{\sigma}_1 \times \vec{\sigma}_2) \cdot \vec{p} (\vec{\tau}_1 + \vec{\tau}_2) \cdot \vec{\chi}^* \\ &+ \frac{\mathcal{B}}{2} (\vec{\sigma}_1 + \vec{\sigma}_2) \cdot \vec{p} (i\vec{\tau}_1 - i\vec{\tau}_2 + \vec{\tau}_1 \times \vec{\tau}_2) \cdot \vec{\chi}^* . \end{aligned} \quad (\text{A.1})$$

with  $\vec{\chi}$  the three–component isospin wave function of the final state pion, e.g.  $\vec{\chi} = (0, 0, 1)$  for  $\pi^0$ –production and  $\vec{\chi} = (1, i, 0)/\sqrt{2}$  for  $\pi^+$ –production. The complex amplitude  $\mathcal{A}$  belongs to the (singlet) transition  ${}^3P_0 \rightarrow {}^1S_0s$  with conserved total isospin  $I_{\text{tot}} = 1$ . Similarly, the complex amplitude  $\mathcal{B}$  belongs to the (triplet) transition  ${}^3P_1 \rightarrow {}^3S_1s$ , also with total isospin  $I_{\text{tot}} = 1$ . In fact the selection rules which follow from the conservation of parity, angular momentum and isospin allow only for these two transitions. Note also that there is an invariance under the substitution  $(\mathcal{A}, \vec{\sigma}_1, \vec{\sigma}_2, \vec{p}) \leftrightarrow (\mathcal{B}, \vec{\tau}_1, \vec{\tau}_2, \vec{\chi}^*)$ .

In the case of (isoscalar) eta production one has,

$$\begin{aligned} \text{T}_{\text{th}}^{\text{cm}}(NN \rightarrow NN\eta) &= \frac{\mathcal{C}}{4} (i\vec{\sigma}_1 - i\vec{\sigma}_2 + \vec{\sigma}_1 \times \vec{\sigma}_2) \cdot \vec{p} (3 + \vec{\tau}_1 \cdot \vec{\tau}_2) \\ &+ \frac{\mathcal{D}}{4} (i\vec{\sigma}_1 - i\vec{\sigma}_2 - \vec{\sigma}_1 \times \vec{\sigma}_2) \cdot \vec{p} (1 - \vec{\tau}_1 \cdot \vec{\tau}_2) . \end{aligned} \quad (\text{A.2})$$

Again, the complex amplitude  $\mathcal{C}$  belongs to the (singlet) transition  ${}^3P_0 \rightarrow {}^1S_0s$  with total isospin  $I_{\text{tot}} = 1$  and the complex amplitude  $\mathcal{D}$  belongs to the (triplet) transition  ${}^1P_1 \rightarrow {}^3S_1s$  with total isospin  $I_{\text{tot}} = 0$ . The determination of the latter amplitude  $\mathcal{D}$  requires measurements of the total cross sections for the process  $pn \rightarrow pn\eta$  having neutrons either in the target or the beam. Finally, we note that the expressions for  $\text{T}_{\text{th}}^{\text{cm}}(NN \rightarrow NN\pi)$  and  $\text{T}_{\text{th}}^{\text{cm}}(NN \rightarrow NN\eta)$  incorporate the Pauli exclusion principle, since combined left–multiplication with the spin–exchange operator  $(1 + \vec{\sigma}_1 \cdot \vec{\sigma}_2)/2$  and the isospin–exchange operator  $(1 + \vec{\tau}_1 \cdot \vec{\tau}_2)/2$  reproduces them up to an important minus sign.

For the sake of completeness, we give also the contributions of the one–boson exchange diagrams discussed in section 5.2 to the (triplet)  $\eta$ –production amplitude  $\mathcal{D}$ . From pseudoscalar meson ( $\pi, \eta$ ) exchange one finds,

$$\mathcal{D}^{(\pi)} = -3\mathcal{C}^{(\pi^0)} = -0.52 \text{ fm}^4 , \quad \mathcal{D}^{(\eta)} = \mathcal{C}^{(\eta, \text{dir})} + \mathcal{C}^{(\eta, \text{res})} = 0.42 \text{ fm}^4 , \quad (\text{A.3})$$

(see Eqs.(49,50,55)). In addition vector meson ( $\rho, \omega$ ) exchange gives rise to the terms,

$$\mathcal{D}^{(\omega)} = \frac{2M + m_\eta}{2M - m_\eta} \mathcal{C}^{(\omega)} = 0.41 \text{ fm}^4 , \quad (\text{A.4})$$

$$\begin{aligned} \mathcal{D}^{(\rho)} &= \frac{3g_{\eta N}g_{\rho N}^2}{2M(M_\rho^2 + Mm_\eta)(2M + m_\eta)} \\ &\times \left[ -2 + \frac{m_\eta}{M}(\kappa_\rho^2 + \kappa_\rho - 1) + \frac{m_\eta^2}{M^2}\kappa_\rho \left(1 + \frac{7}{8}\kappa_\rho\right) \right] = 1.50 \text{ fm}^4 , \end{aligned} \quad (\text{A.5})$$

(see Eq.(51)). These contributions sum up to  $\mathcal{D}^{(\text{thy})} = 1.81 \text{ fm}^4$ . The expression for the total cross section  $\sigma_{\text{tot}}(T_{\text{lab}})$  of the reaction  $pn \rightarrow pn\eta$  is obtained from Eq.(45) replacing the factor  $2|\mathcal{C}|^2 F_p(W)$  by  $|\mathcal{C}|^2 F_s(W) + |\mathcal{D}|^2 F_t(W)$  (see Eq.(31)) and we have neglected the small neutron–proton mass difference.

Recently, total cross sections for  $pn \rightarrow pn\eta$  have been extracted from measurements of the process  $pd \rightarrow ppn\eta$  at CELSIUS [55]. A fit of the two data points closest to threshold (at  $T_{\text{lab}} = 1296$  and  $1322 \text{ MeV}$ ) gives for the empirical triplet  $\eta$ –production amplitude  $|\mathcal{D}|^{(\text{exp})} = 2.3 \text{ fm}^4$ . Compared to this value the abovementioned theoretical prediction,  $\mathcal{D}^{(\text{thy})} = 1.8 \text{ fm}^4$ , is only about 20% too small.

## B Imaginary parts from one–pion loop graphs

In this appendix we will give explicit expressions for the imaginary parts of the pion production threshold amplitudes  $\text{Im } \mathcal{A}$  and  $\text{Im } \mathcal{B}$  as they arise in one–pion loop approximation. To that order any non–vanishing imaginary part can only come from those one–loop diagrams which involve proton rescattering in the initial state. These are just the two–pion exchange box diagrams shown in Fig. 9. We apply the Cutkosky cutting rules to evaluate their imaginary part. It is then given by the product of the upper tree–level subgraph (i.e. the threshold pion production amplitude with  $1\pi$ –exchange including the leading order isovector pion rescattering) and of one–half the invariant  $pp$  two-body phase space times the lower tree–level subgraph. The latter two factors combine to the  ${}^3P_0$  or  ${}^3P_1$   $pp$  phase shift calculated perturbatively in  $1\pi$ –exchange approximation at  $T_{\text{lab}}^{\text{th}} = m_\pi(2 + m_\pi/2M)$ . Altogether one gets thus from perturbative unitarity,

$$\text{Im } \mathcal{A} = \mathcal{A}^{(\pi, \text{dir})} \cdot \delta_{1\pi}({}^3P_0) , \quad (\text{B.1})$$

$$\text{Im } \mathcal{B} = \left( \mathcal{B}_{|c_4=0}^{(\pi, \text{iv})} + \mathcal{B}^{(\pi, \text{dir})} \right) \cdot \delta_{1\pi}({}^3P_1) , \quad (\text{B.2})$$

with  $\mathcal{A}^{(\pi, \text{dir})}$ ,  $\mathcal{B}_{|c_4=0}^{(\pi, \text{iv})}$  and  $\mathcal{B}^{(\pi, \text{dir})}$  given in Eqs.(12,34,35). Using the projection formulas of ref.[34] to calculate the  $1\pi$ –exchange  ${}^3P_{0,1}$  phase shifts one finds the following analytical results,

$$\text{Im } \mathcal{A} = \frac{g_{\pi N}^5 \sqrt{\mu(4 + \mu)}}{64\pi M^4 (1 + \mu)(2 + \mu)^2} \left[ 1 - \frac{\mu}{4 + \mu} \ln \left( 2 + \frac{4}{\mu} \right) \right] = 0.54 \text{ fm}^4 , \quad (\text{B.3})$$

$$\begin{aligned} \text{Im } \mathcal{B} &= \frac{g_{\pi N}^5 \sqrt{\mu(4 + \mu)}}{64\pi M^4 (1 + \mu)(2 + \mu)^2} \left( 3 + 2\mu - 2g_A^{-2}(2 + \mu) \right) \\ &\times \left[ \frac{\mu - 4}{2(4 + \mu)} - \frac{\mu^2}{(4 + \mu)^2} \ln \left( 2 + \frac{4}{\mu} \right) \right] = -0.24 \text{ fm}^4 , \end{aligned} \quad (\text{B.4})$$

with  $g_A = g_{\pi N} f_\pi / M$ . One observes that in one–pion loop approximation  $\text{Im } \mathcal{A}$  is too large by a factor of 2 with the wrong (positive) sign, whereas  $\text{Im } \mathcal{B}$  is too small by a factor of 6. Clearly, there is important short range NN–dynamics missing in one–pion loop approximation as can be seen by comparing the empirical  ${}^3P_{0,1}$  phase shifts at  $T_{\text{lab}}^{\text{th}} = m_\pi(2 + m_\pi/2M)$ ,  $\delta({}^3P_0) = -6.3^\circ$  and  $\delta({}^3P_1) = -28.1^\circ$ , with the  $1\pi$ –exchange approximation,  $\delta_{1\pi}({}^3P_0) = +65.0^\circ$  and  $\delta_{1\pi}({}^3P_1) = -34.6^\circ$ . If one considers all those one–loop box diagrams which include in the

upper part all tree graphs evaluated in section 4.2 and in the lower part only the one-pion exchange one gets for the imaginary part of  $\mathcal{B}$ ,

$$\text{Im } \mathcal{B} = \mathcal{B}^{(\text{thy})} \cdot \delta_{1\pi}(^3P_1) = 2.74 \text{ fm}^4 \cdot (-0.604) = -1.65 \text{ fm}^4 , \quad (\text{B.5})$$

a value which is in 10% agreement with the empirical  $\text{Im } \mathcal{B} = -1.5 \text{ fm}^4$ . Of course, this merely reflects the fact that the empirical  $^3P_1$  phase shift at  $T_{\text{lab}}^{\text{th}}$  is not far from one obtained in  $1\pi$ -exchange approximation. Note, however, that for the  $^3P_0$  phase shift at  $T_{\text{lab}}^{\text{th}}$  the empirical value and the  $1\pi$ -exchange approximation differ by a large factor of  $-10$ .

## C Effective field theory approach to final-state interaction

In this appendix we want to give an elementary derivation of the final-state interaction correction factor Eq.(6),  $F_p(W) = [1 + a_p^2 P_*^2]^{-1}$ ,  $P_*^2 = W^2/4 - M^2$ , in scattering length approximation (i.e. for  $r_p = 0$ ). Close to threshold all final state three-momenta are small and therefore one can approximate both the meson production process  $NN \rightarrow NN\pi^0$  and elastic  $NN \rightarrow NN$  scattering by momentum independent contact vertices proportional to  $\mathcal{A}$  and the scattering length  $a_p$ , respectively. Consider first low energy  $NN$ -scattering in this approximation. The bubble diagrams with  $0,1,2,\dots$  rescatterings can be easily summed up in the form of a geometric series,

$$a_p - 4\pi a_p^2 \int \frac{d^3l}{(2\pi)^3} \frac{1}{P_*^2 + i0^+ - l^2} + \dots = a_p + i a_p^2 P_* + \dots = \frac{a_p}{1 - i a_p P_*} , \quad (\text{C.1})$$

using dimensional regularization to evaluate the (vanishing) real part of the loop integral. Obviously, the sum of these infinitely many loop diagrams is just the unitarized scattering length approximation which leads to,

$$\tan \delta_0(W) = a_p P_* . \quad (\text{C.2})$$

Next, consider in the same approximation meson production followed by an arbitrary number of  $NN$ -rescatterings in the final-state. Again, these loop diagrams can be summed up to,

$$\frac{\mathcal{A}}{1 - i a_p P_*} , \quad (\text{C.3})$$

and taking the absolute square,

$$\left| \frac{\mathcal{A}}{1 - i a_p P_*} \right|^2 = \frac{|\mathcal{A}|^2}{1 + a_p^2 P_*^2} , \quad (\text{C.4})$$

one encounters the final-state interaction correction factor  $F_p(W) = [1 + a_p^2(W^2/4 - M^2)]^{-1}$  in scattering length approximation. Since, the scattering length is much bigger than the effective range parameter for  $NN$ -scattering ( $a_p \gg r_p$ ) one has already derived the dominant effect due to final-state interaction. Of course, in order to be more accurate one should eventually go beyond momentum independent contact vertices. The main point we want to make here is that the final-state interaction correction factor  $F_p(W)$  (for  $r_p = 0$ ) has a sound foundation in effective field theory.

## References

- [1] H.O. Meyer et al., Phys. Rev. Lett. 65 (1990) 2846; Nucl. Phys. A539 (1992) 663.
- [2] A. Bondar et al., Phys. Lett. B356 (1995) 8.
- [3] M. Drochner et al., Phys. Rev. Lett. 77 (1996) 454;  
C. Heimberg et al., Phys. Rev. Lett. 77 (1996) 1012.
- [4] J.G. Hardie et al., Phys. Rev. C56 (1997) 20.
- [5] H. Calen et al., Phys. Lett. B366 (1996) 39.
- [6] G. Miller and P. Sauer, Phys. Rev. C44 (1991) 1725.
- [7] T.-S.H. Lee and D.O. Riska, Phys. Rev. Lett. 70 (1993) 2237.
- [8] C.J. Horowitz, H.O. Meyer and D.K. Griegel, Phys. Rev. C49 (1994) 1337.
- [9] E. Hernandez and E. Oset, Phys. Lett. B350 (1995) 158.
- [10] C. Hanhart, J. Haidenbauer, A. Reuber, C. Schütz and J. Speth, Phys. Lett. B358 (1995) 21.
- [11] B.Y. Park, F. Myhrer, J.R. Morones, T. Meissner and K. Kubodera, Phys. Rev. C53 (1996) 1519.
- [12] T.D. Cohen, J.L. Friar, G.A. Miller and U. van Kolck, Phys. Rev. C53 (1996) 2661.
- [13] U. van Kolck, G.A. Miller and D.O. Riska, Phys. Lett. B388 (1996) 679.
- [14] T. Sato, T.-S.H. Lee, F. Myhrer and K. Kubodera, Phys. Rev. C56 (1997) 1246.
- [15] C. Hanhart, J. Haidenbauer, M. Hoffmann, Ulf-G. Meißner and J. Speth, Phys. Lett. B424 (1998) 8.
- [16] E. Gedalin, A. Moalem and L. Razdolskaya, [nucl-th/9803029].
- [17] M.E. Schillaci, R.E. Silbar and J.E. Young, Phys. Rev. 179 (1969) 1539.
- [18] V. Bernard, N. Kaiser and Ulf-G. Meißner, Nucl. Phys. B475 (1995) 147.
- [19] V. Bernard, N. Kaiser, Ulf-G. Meißner and A. Schmidt, Nucl. Phys. A580 (1994) 475;  
V. Bernard, N. Kaiser and Ulf-G. Meißner, Phys. Lett. B382 (1996) 19.
- [20] V. Bernard, N. Kaiser and Ulf-G. Meißner, Nucl. Phys. A619 (1997) 261.
- [21] K.M. Watson, Phys. Rev. 88 (1952) 1163.
- [22] O. Dumbrajs et al., Nucl. Phys. B216 (1983) 277.
- [23] J. Adam, A. Stadler, M.T. Pena and F. Gross, Phys. Lett. B407 (1997) 97.
- [24] J. Gasser, M.E. Sainio and A. Švarc, Nucl. Phys. B307 (1988) 779.
- [25] V. Bernard, N. Kaiser and Ulf-G. Meißner, Nucl. Phys. A615 (1997) 483.
- [26] V. Bernard, N. Kaiser and Ulf-G. Meißner, Int.J. Mod. Phys. E4 (1995) 193.
- [27] P. Mergell, Ulf-G. Meißner and D. Drechsel, Nucl. Phys. A596 (1996) 367.
- [28] W. Grein and P. Kroll, Nucl. Phys. A338 (1980) 332; Nucl. Phys. A377 (1982) 505.
- [29] K. Holinde, Prog. Part. Nucl. Phys. 36 (1996) 311.
- [30] Ulf-G. Meißner, V. Mull, J. Speth and J.W. Van Orden, Phys. Lett. B408 (1997) 381.
- [31] G. Höhler and E. Pietarinen, Nucl. Phys. B95 (1975) 210.
- [32] P. Jain, R. Johnson, Ulf-G. Meißner, N.W. Park and J. Schechter, Phys. Rev. D37 (1988) 3252.
- [33] F. Klingl, N. Kaiser and W. Weise, Z. Phys. A356 (1996) 193.
- [34] N. Kaiser, R. Brockmann and W. Weise, Nucl. Phys. A625 (1997) 758.

- [35] K.Th. Brinkmann (for the COSY-TOF collaboration), Proceedings of the workshop "Meson 98", Krakow, Poland; Act. Phys. Pol., in print.
- [36] A. Engel, R. Shyam, U. Mosel and A.K. Dutt–Mazumder, Nucl. Phys. A603 (1996) 387.
- [37] R. Shyam and U. Mosel, Phys. Lett. B426 (1998) 1.
- [38] M. Batinic, I. Slaus, A. Svarc and B.M.K. Nefkens, Phys. Rev. C51 (1995); (E) Phys. Rev. C57 (1998) 1004; M. Batinic, I. Dadic, I. Slaus, A. Svarc, B.M.K. Nefkens and T.-S.H. Lee, Physica Scripta 58 (1998) 15. The value for  $a_{\eta N}$  is taken from the last reference.
- [39] D. Sigg et al., Nucl. Phys. A609 (1996) 269; (E) Nucl. Phys. A617 (1997) 526.
- [40] A.M. Green and S. Wycech, Phys. Rev. C55 (1997) R2167.
- [41] E. Chiavassa et al., Phys. Lett. B322 (1994) 270.
- [42] A.M. Bergdolt et al., Phys. Rev. D48 (1993) R2969.
- [43] F. Hibou et al., [nucl-ex/9802002] (to be published).
- [44] H. Calen et al., [nucl-ex/9811003].
- [45] M. Bourquin et al., Z. Phys. C21 (1983) 27.
- [46] P.G. Ratcliffe. Phys. Lett. B365 (1996) 383.
- [47] R. Machleidt, K. Holinde and C. Elster, Phys. Rep. 149 (1987) 1.
- [48] G. Ecker, J. Gasser, A. Pich and E. de Rafael, Nucl. Phys. B321 (1989) 311.
- [49] A. Moalem et al., Nucl. Phys. A589 (1995) 649; Nucl. Phys. A600 (1996) 445; Nucl. Phys. A634 (1998) 368.
- [50] G. Fäldt and C. Wilkin, Nucl. Phys. A604 (1995) 441; Z. Phys. A357 (1997) 241.
- [51] P. Moskal et al., Phys. Rev. Lett. 80 (1998) 3202.
- [52] A.V. Efremov, J. Soffer and N.A. Törnqvist, Phys. Rev. D44 (1991) 1369.
- [53] G. Altarelli, R.D. Ball, S. Forte and G. Ridolfi, Nucl. Phys. B496 (1997) 337.
- [54] A. Sibirtsev and W. Cassing, Eur. J. Phys. A2 (1998) 333.
- [55] H. Calen et al., Phys. Rev. C58 (1998) 2667.

## Figures

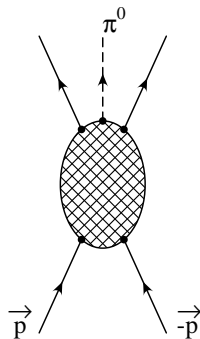


Figure 1: The process  $pp \rightarrow pp\pi^0$  in the center-of-mass system.

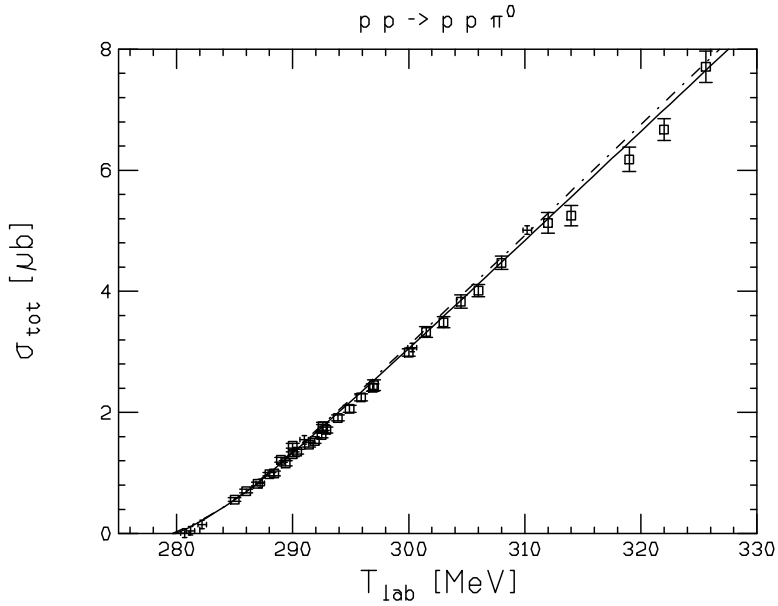


Figure 2: Fit to the total cross section for  $pp \rightarrow pp\pi^0$  as described in the text (solid line). The data are from [1] (boxes) and [2] (crosses). The dashed line is explained in sec. 3.4.

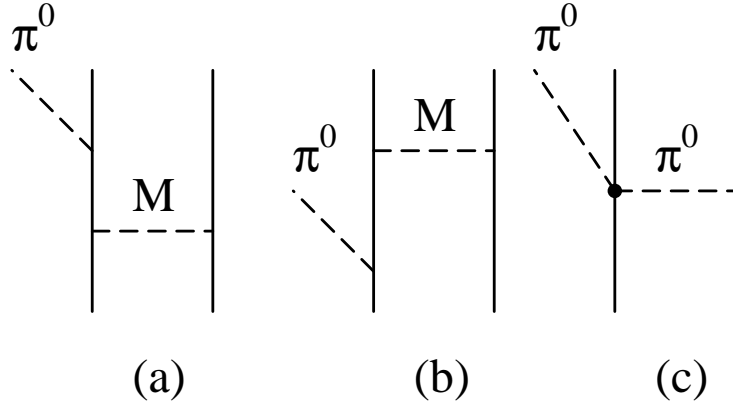


Figure 3: Feynman graphs for neutral pion production. (a) and (b) are the direct terms, with meson exchange  $\mathcal{M} = \pi^0, \eta, \omega, \rho^0$ . (c) is the rescattering graph. The heavy dot denotes the second order isoscalar chiral  $\pi\pi NN$ -vertex. Graphs where the pion (dashed line) is emitted from the other proton (solid) line and graphs with crossed outgoing proton lines are not shown.

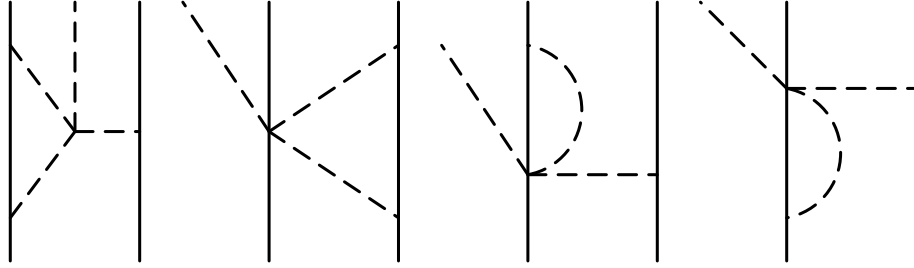


Figure 4: Class of one loop graphs involving the  $\pi\pi$  interaction. For further notation, see Fig.3.

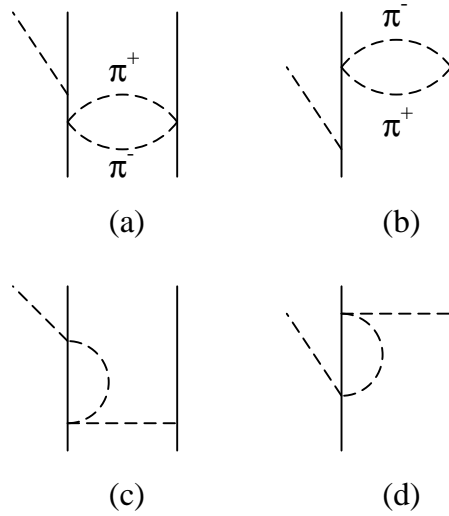


Figure 5: Further loop diagrams proportional to  $g_{\pi N}/f_{\pi}^4$ . (a) and (b) represent  $\pi^+\pi^-$  exchange between protons, (c) and (d) are the  $\pi^+$  rescattering diagrams. For further notation, see Fig.3.

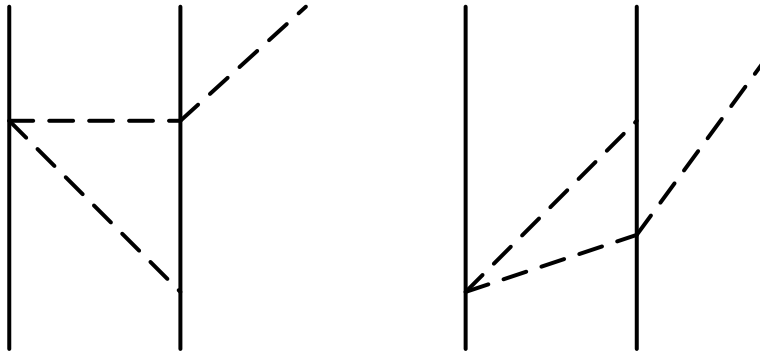


Figure 6: Loop diagrams with  $\pi^0$  emission via charge exchange. For further notation, see Fig.3.

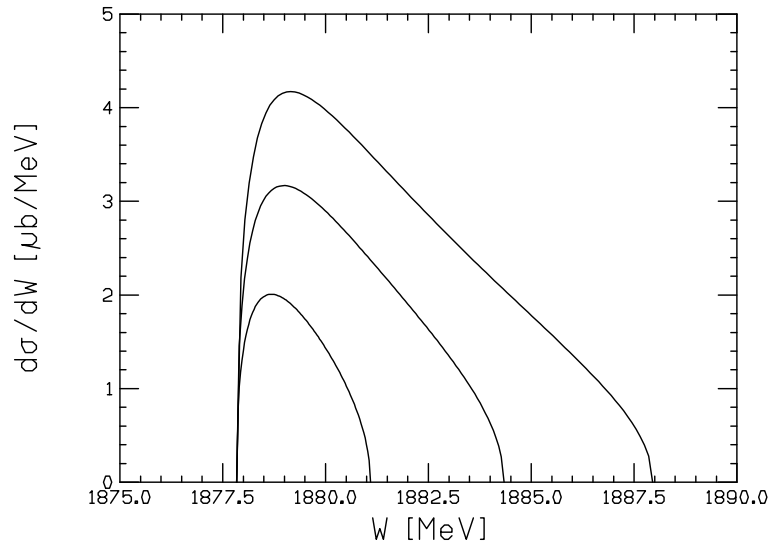


Figure 7: Pion production cross section as a function of the  $pn$  invariant mass  $W$ . The three curves corresponds to  $T_{\text{lab}} = 299.3, 306.3$  and  $314.1$  MeV, in ascending order.

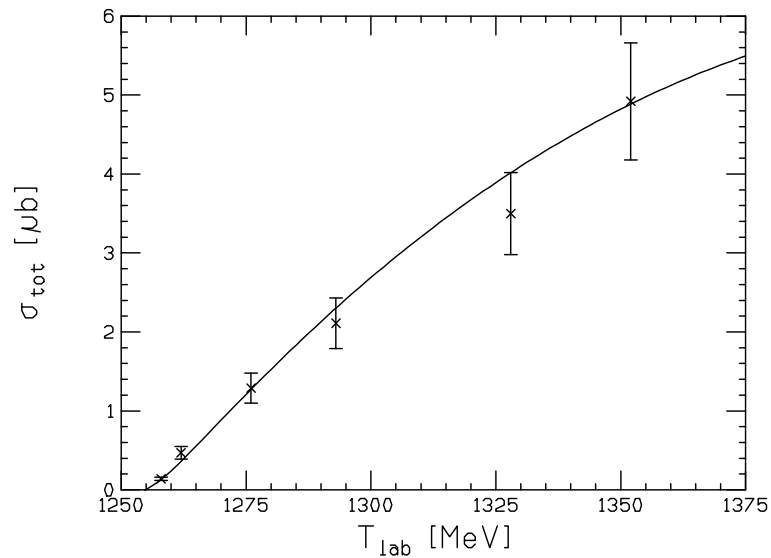


Figure 8: The eta-production cross section  $\sigma_{\text{tot}}(pp \rightarrow pp\eta)$  as a function of  $T_{\text{lab}}$ . The data are taken from ref.[5].

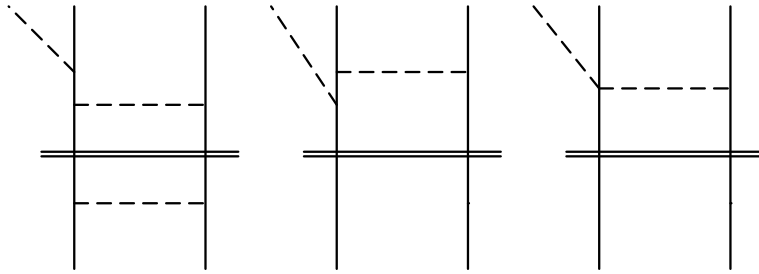


Figure 9: Diagrams that give rise to the non-vanishing imaginary parts  $\text{Im } \mathcal{A}$  and  $\text{Im } \mathcal{B}$  in one-pion loop approximation. The projection on the on-shell  $pp$  intermediate state is symbolized by the double line cutting the diagrams. For further notation, see Fig. 3.